Part 2

Optical Properties of Bulk Matter

Chapter 9

Classical Theories of Optical Constants

A new silver coin or a polished aluminum cooking pan is shiny but opaque to transmitted light; pure water or a piece of window glass is transparent but weakly reflecting; the light transmitted by ruby gemstones is red. Such commonly observed phenomena are consequences of the many different ways in which objects reflect and transmit visible light; but these properties are determined by the more fundamental optical constants of the materials of which the objects are composed. Relations between optical constants and reflection and transmission at plane interfaces were derived in Chapter 2. In this chapter we show how the variation of optical constants can be understood by appealing to simple models of the microscopic structure of matter.

There are two sets of quantities that are often used to describe optical properties: the real and imaginary parts of the *complex refractive index* $N = n + ik$ and the real and imaginary parts of the *complex dielectric function* (or relative permittivity) $\epsilon = \epsilon' + i\epsilon''$. These two sets of quantities are not independent; either may be thought of as describing the intrinsic optical properties of matter. The relations between the two are, from (2.47) and (2.48),

$$\epsilon' = \frac{\varepsilon'}{\varepsilon_0} = n^2 - k^2,$$
$$\epsilon'' = \frac{\varepsilon''}{\varepsilon_0} = 2nk, \tag{9.1}$$

$$n = \sqrt{\frac{\sqrt{\epsilon'^2 + \epsilon''^2} + \epsilon'}{2}},$$

$$k = \sqrt{\frac{\sqrt{\epsilon'^2 + \epsilon''^2} - \epsilon'}{2}}, \tag{9.2}$$

where we have assumed that the material is nonmagnetic ($\mu = \mu_0$).

In Part 2 we shall usually give both sets of optical constants, (n, k) and (ϵ', ϵ''), side by side. For some purposes one set is preferable, and for other

purposes the other set is preferred. For example, most people have a better intuitive understanding of n and k because they are related to the phase velocity and attenuation of plane waves in matter. In considerations of wave propagation, therefore, n and k are preferred. However, in considering the microscopic mechanisms that are responsible for optical effects, ϵ' and ϵ'' are more appropriate. Reflection and transmission by slabs and plane interfaces are described more simply with n and k, while equations for absorption and scattering by particles small compared with the wavelength are more simply written using ϵ' and ϵ''. Therefore, at the slight risk of undue repetition, we shall display both sets of optical constants.

9.1 THE LORENTZ MODEL

Near the beginning of this century H. A. Lorentz developed a classical theory of optical properties in which the electrons and ions of matter were treated as simple harmonic oscillators (i.e., "springs") subject to the driving force of applied electromagnetic fields. The results obtained therefrom are formally identical to those of quantum-mechanical treatments, although various quantities are interpreted differently in the classical and quantum-mechanical theories. As most of us are more comfortable thinking in classical terms, it is fortunate that we may do so without doing violence to the correct results. This undoubtedly explains why the Lorentz model remains so useful, not only in guiding our intuition, but also in quantitatively analyzing experimental data.

Following Lorentz, we take as our microscopic model of polarizable matter a collection of identical, independent, isotropic harmonic oscillators (Fig. 9.1). We shall later generalize to more than one kind of oscillator and to anisotropic oscillators. An oscillator with mass m and charge e is acted upon by: a linear restoring force $K\mathbf{x}$, where K is the spring constant (stiffness) and $\mathbf{x}$ is the displacement from equilibrium; a damping force $b\dot{\mathbf{x}}$, where b is the damping constant; and a driving force produced by the *local* electric field $\mathbf{E}_{\text{local}}$ (magnetic forces may usually be neglected compared with electrical forces). We neglect radiation reaction. The equation of motion of such an oscillator is

$$m\ddot{\mathbf{x}} + b\dot{\mathbf{x}} + K\mathbf{x} = e\mathbf{E}_{\text{local}}. \tag{9.3}$$

The *local field* $\mathbf{E}_{\text{local}}$ "seen" by a single oscillator and the *macroscopic field* $\mathbf{E}$, which is an average over a region containing many oscillators, are different in general. However, we shall ignore this difference because it does not affect our simple model of optical constants, and proper treatment of the local field would be a fruitless digression at this point. A good elementary discussion of the local field is given in Kittel (1971, pp. 454–458).

The electric field is taken to be time harmonic with frequency ω. As in previous chapters, we shall deal with the complex representations of the real

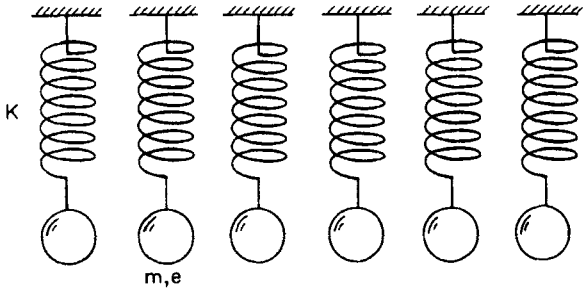

Figure 9.1 The Lorentz model of matter.

time-harmonic quantities (see Section 2.2). The solution to (9.3) is composed of a transient part, which dies away because of damping, and an oscillatory part with the same frequency as the driving field. We shall be interested only in the oscillatory part

$$\mathbf{x} = \frac{(e/m)\mathbf{E}}{\omega_0^2 - \omega^2 - i\gamma\omega}, \tag{9.4}$$

where $\omega_0^2 = K/m$ and $\gamma = b/m$. If $\gamma \neq 0$, the proportionality factor between $\mathbf{x}$ and $\mathbf{E}$ is complex; therefore, the displacement and field are not, in general, in phase. In order to discuss the consequences of this phase difference, we write the displacement as $Ae^{i\Theta}(e\mathbf{E}/m)$, where the amplitude A and phase angle Θ are

$$A = \frac{1}{\left[\left(\omega_0^2 - \omega^2\right)^2 + \gamma^2\omega^2\right]^{1/2}},$$

$$\Theta = \tan^{-1}\frac{\gamma\omega}{\omega_0^2 - \omega^2}. \tag{9.5}$$

These are shown as functions of frequency in Fig. 9.2*a*. Note that the amplitude is a maximum at $\omega \simeq \omega_0$, where the height of this maximum is inversely proportional to γ, and the width at half-maximum is proportional to γ (provided that $\gamma \ll \omega_0$). At low frequencies ($\omega \ll \omega_0$) the oscillator responds in phase with the driving force ($\Theta \simeq 0^0$), whereas at high frequencies ($\omega \gg \omega_0$) the two are 180° out of phase; the 180° phase change occurs in the vicinity of the resonant frequency ω_0. The behavior of the phase will be helpful in understanding the speed of light in matter.

Given the response of a single oscillator to a time-harmonic electric field, the optical constants appropriate to a collection of such oscillators readily follow. The induced dipole moment $\mathbf{p}$ of an oscillator is $e\mathbf{x}$. If $\mathcal{N}$ is the number of oscillators per unit volume, the polarization $\mathbf{P}$ (dipole moment per unit

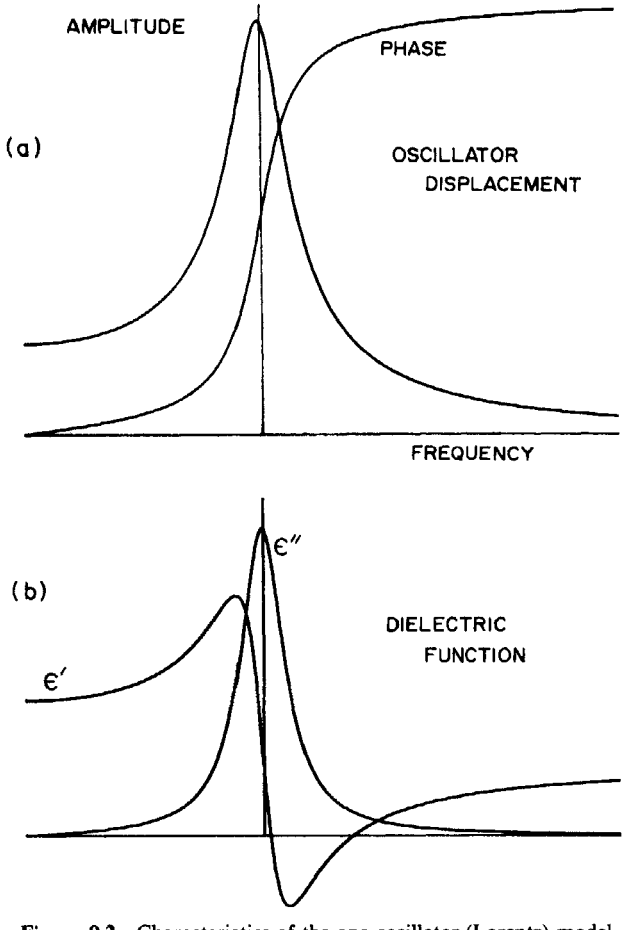

Figure 9.2 Characteristics of the one-oscillator (Lorentz) model.

volume) is $\mathcal{N}\mathbf{p} = \mathcal{N}e\mathbf{x}$, and from (9.4) we have

$$\mathbf{P} = \frac{\omega_p^2}{\omega_0^2 - \omega^2 - i\gamma\omega}\varepsilon_0\mathbf{E}, \tag{9.6}$$

where the *plasma frequency* is defined by $\omega_p^2 = \mathcal{N}e^2/m\varepsilon_0$. Equation (9.6) is a particular example of the constitutive relation (2.9). Therefore, the dielectric function for our system of simple harmonic oscillators is

$$\epsilon = 1 + \chi = 1 + \frac{\omega_p^2}{\omega_0^2 - \omega^2 - i\gamma\omega}, \tag{9.7}$$

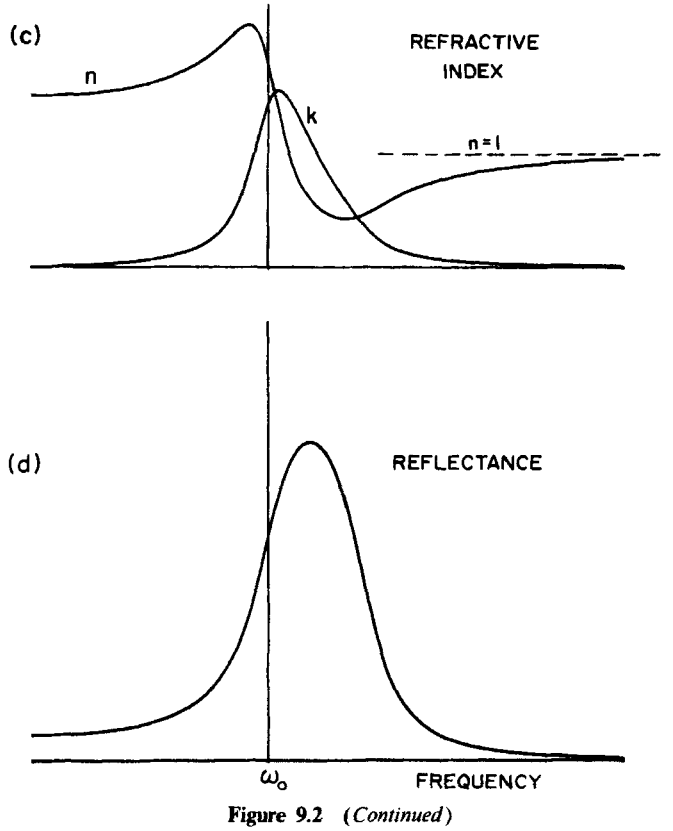

Figure 9.2 *(Continued)*

with real and imaginary parts

$$\epsilon' = 1 + \chi' = 1 + \frac{\omega_p^2(\omega_0^2 - \omega^2)}{(\omega_0^2 - \omega^2)^2 + \gamma^2\omega^2}, \tag{9.8}$$

$$\epsilon'' = \chi'' = \frac{\omega_p^2\gamma\omega}{(\omega_0^2 - \omega^2)^2 + \gamma^2\omega^2}. \tag{9.9}$$

The proof is lengthy, although straightforward, and will be omitted here, but it can be shown by direct substitution and integration that χ' and χ'' satisfy the Kramers–Kronig relations (2.36) and (2.37).

The frequency dependence of the real and imaginary parts of the dielectric function (9.7) are shown schematically in Fig. 9.2*b*; following this are the corresponding real and imaginary parts of the refractive index (Fig. 9.2*c*). The reflectance at normal incidence (2.58) is also of interest and is shown in Fig. 9.2*d*. Many features of the optical properties of materials are illustrated by

these characteristics of the simple oscillator model because such an oscillator can describe many different kinds of optical excitations. Several examples of actual data will be compared with the results of the oscillator model later in the chapter. First, however, there are some general oscillator characteristics that should be noted:

The region of high absorption at frequencies around ω_0 gives rise to an associated region of high reflectance provided, of course, that the oscillator parameters are such that $k \gg 1$ in this region. The high reflectance allows little light to get past the bounding surface of the material, and that which does is rapidly attenuated.

On both sides of the resonance region n increases with increasing frequency, which is called *normal dispersion*. Only in the immediate vicinity of the resonance frequency does n decrease with frequency, so-called *anomalous dispersion*. Such a reversal of dispersion, if it occurred in transparent regions, would provide a much-needed material for designing color-corrected lenses. Unfortunately, anomalous dispersion occurs only in regions of high absorption where no appreciable light is transmitted.

The maximum value of ϵ'' occurs approximately at ω_0 provided that $\gamma \ll \omega_0$. For frequencies in the neighborhood of ω_0 the dielectric functions (9.8) and (9.9) may be approximated by

$$\epsilon' \simeq 1 + \frac{\omega_p^2(\omega_0 - \omega)/2\omega_0}{(\omega_0 - \omega)^2 + (\gamma/2)^2}, \tag{9.10}$$

$$\epsilon'' \simeq \frac{\gamma\omega_p^2/4\omega_0}{(\omega_0 - \omega)^2 + (\gamma/2)^2}. \tag{9.11}$$

It is obvious from (9.11) that the maximum value of ϵ'' is approximately $\omega_p^2/\gamma\omega_0$ and the width of the bell-shaped curve $\epsilon''(\omega)$ is γ (i.e., ϵ'' falls to one-half its maximum value when $\omega_0 - \omega = \pm\gamma/2$). If we set the derivative of (9.10) with respect to the variable $\omega_0 - \omega$ equal to zero, it follows that the extreme values of ϵ', $\epsilon'_{\max} = 1 + \epsilon''_{\max}/2$ and $\epsilon'_{\min} = 1 - \epsilon''_{\max}/2$, occur at $\omega = \omega_0 - \gamma/2$ and $\omega = \omega_0 + \gamma/2$, respectively. These properties of a narrow Lorentzian line are very helpful in quickly visualizing the shape of $\epsilon(\omega)$ from the parameters of (9.7).

9.1.1 Comparison of Classical and Quantum-Mechanical Concepts

The models of optical properties in this book are strictly classical. However, modern theoretical work aimed at understanding in detail the microphysics of optical properties is mostly quantum mechanical. Therefore, in this section we briefly discuss a few relevant quantum-mechanical concepts and also show that there is an analogy between the classical and quantum-mechanical descriptions of optical properties.

Most readers are no doubt comfortable with the alternative descriptions of light as either a stream of *photons*—quanta of electromagnetic energy—or electromagnetic *waves*. The relation between the two is $\mathcal{E} = \hbar\omega$, where ω is the angular frequency of the electromagnetic wave, $\mathcal{E}$ is the energy of the associated photon, and $\hbar$ is Planck's constant divided by 2π. In discussing the interaction of photons with matter, we must acknowledge that they do so in a discrete manner: a photon absorbed in matter gives up its energy and momentum to produce quantum *excitations*. Each excitation has its own quantized energy and momentum. A large part of the research effort in solid-state physics is involved with investigating the spectrum of such elementary excitations.

One important example is the *phonon*, a quantum of lattice vibration. An incident photon may give up its energy in a solid and create a phonon in the process. A less likely outcome is the production of two or more phonons within the bounds imposed by energy and momentum conservation. It is also possible for a photon to interact in a solid by exciting a phonon of lesser energy, the energy difference being carried off by another photon; such processes, called *inelastic*, include Raman and Brillouin scattering and are beyond the scope of this book. The following is a partial list of quantum excitations; we shall discuss some of these later.

Phonon	quantized lattice wave
Plasmon	quantized plasma (charge density) wave
Magnon	quantized magnetic spin wave
Exciton	quantum of electronic excitation consisting of an electron–hole pair
Polariton	quantum of coupled electromagnetic wave and another excitation such as a phonon or plasmon

The quantum-mechanical expression for the dielectric function may be written in the form (see, e.g., Ziman, 1972, Chap. 8, for an elementary discussion of the quantum theory of optical properties)

$$\epsilon(\omega) = 1 + \sum_j \frac{(\mathcal{N}e^2/m\epsilon_0)f_{ij}}{\omega_{ij}^2 - \omega^2 - i\gamma_j\omega}. \tag{9.12}$$

Note that if $j = 1$, (9.12) is *formally* identical with the classical expression (9.7); the classical multiple oscillator model, which will be discussed in Section 9.2, is even more closely analogous to (9.12). However, the *interpretations* of the terms in the quantum and classical expressions are quite different. Classically, ω_0 is the resonance frequency of the simple harmonic oscillator; quantum mechanically ω_{ij} is the energy difference (divided by $\hbar$) between the initial or ground state i and excited state j. Classically, γ is a damping factor such as that caused by drag on an object moving in a viscous fluid; quantum mechanically, γ_j

relates to the probabilities of transition to all other quantum states. The *oscillator strengths* f_{ij} represent the probability of an excitation from state i to state j; they are calculated through the matrix elements of the dipole moment operator. Despite considerable underlying conceptual differences, the formal similarities between the classical and quantum-mechanical theories allow us to think classically and not be far wrong.

9.1.2 High- and Low-Frequency Limiting Behavior

For frequencies much *greater* than the resonance frequency, the real and imaginary parts of the dielectric function (9.7) are approximately

$$\begin{aligned} \epsilon' &\simeq 1 - \frac{\omega_p^2}{\omega^2}, \\ \epsilon'' &\simeq \frac{\gamma\omega_p^2}{\omega^3}. \end{aligned} \qquad \omega \gg \omega_0 \tag{9.13}$$

The real part of the dielectric function approaches unity from below, while the imaginary part tends to zero as the inverse third power of the frequency. The corresponding components of the refractive index are

$$\begin{aligned} n &\simeq \sqrt{\epsilon'} \simeq 1 - \frac{\omega_p^2}{2\omega^2}, \\ k &\simeq \frac{\epsilon''}{2} \simeq \frac{\gamma\omega_p^2}{2\omega^3}, \end{aligned} \qquad \omega \gg \omega_0 \tag{9.14}$$

and the reflectance at normal incidence is, from (9.14) and (2.58),

$$R \simeq \left(\frac{\omega_p}{2\omega}\right)^4 \qquad \omega \gg \omega_0. \tag{9.15}$$

The $1/\omega^4$ high frequency limit for R can be useful in determining optical constants from Kramers–Kronig analysis of reflectance data (see Section 2.7). Reflectances at frequencies higher than the greatest far-ultraviolet frequency for which measurements are made can be calculated from (9.15) and used to complete the Kramers–Kronig integral to infinite frequency.

For frequencies much *less* than the resonance frequency, the real and imaginary parts of (9.7) are

$$\begin{aligned} \epsilon' &\simeq 1 + \frac{\omega_p^2}{\omega_0^2}, \\ \epsilon'' &\simeq \frac{\gamma\omega_p^2\omega}{\omega_0^4} \end{aligned} \qquad \omega \ll \omega_0. \tag{9.16}$$

The imaginary part tends to zero as ω, and the real part approaches a constant that depends on the number density of oscillators and their mass.

Notions of "high"- and "low"-frequency limiting behavior depend on one's point of view, and the notation reflects this: what is low frequency to an ultraviolet spectroscopist may be high frequency to an infrared spectroscopist. For insulating solids the value of ϵ' in the near infrared is often denoted as ϵ_0 by ultraviolet spectroscopists; it refers to frequencies low compared with certain oscillators—electrons in this example—which may, however, be high compared with lattice vibrational frequencies. Consequently, this same limiting value is denoted as ϵ_∞ by infrared workers.

The low-frequency limit of ϵ'' (9.16) correctly describes the far-infrared ($1/\lambda$ less than about 100 cm^{-1}) behavior of many crystalline solids because their strong vibrational absorption bands are at higher frequencies. This limiting value for the bulk absorption, coupled with the absorption efficiency in the Rayleigh limit (Section 5.1), gives an ω^2 dependence for absorption by small particles; this is expected to be valid for many particles at far-infrared wavelengths.

9.1.3 Index of Refraction Less Than 1

When encountered for the first time, a refractive index n less than 1, such as at frequencies greater than ω_0 in Fig. 9.2*c*, often causes great anguish—sometimes followed by heated debate. For one of the consequences of special relativity is that speeds greater than c, the free-space speed of light, are not attainable; yet the phase velocity of a plane harmonic wave is c/n (Section 2.6). In fact, this was used as a stick—to no effect—with which to beat the theory of relativity during its infancy. In elementary texts this problem is sometimes disposed of by invoking the *group velocity* $c/[d(\omega n)/d\omega]$ and stating that it is this velocity which cannot exceed c. This may be so in regions of normal dispersion, but in regions of anomalous dispersion the group velocity can exceed c and, indeed, can be negative. So invoking the group velocity is only likely to compound the anguish.

This apparent clash with special relativity arises from the mistaken assumption that all quantities with dimensions of velocity are constrained to be less than or equal to c. Special relativity only places an upper bound on the velocity of *material bodies*, and we can extend this to mean *signals* as well. The phase velocity of a plane harmonic wave is the velocity of neither a material body nor a signal; an observer equipped with a detector and situated in the medium does not measure c/n as the speed at which the troughs and crests of the wave go by him. The plane wave originates from a source which has been turned on for a sufficient period of time to allow the wave to be established throughout the medium. The only way to measure the velocity of a signal is to turn off the source, note the distance between source and detector, turn on the source, and wait for a response. The distance to the source divided by the time elapsed between turning on the source and noting the first response of the detector

cannot be greater than c. To show this we must consider the propagation of a pulse, which can be decomposed into its Fourier components (Section 2.3), each of which propagates with a different phase velocity—some greater than and some less than c. As a consequence of dispersion—n depends on frequency—the pulse changes its shape in a complicated way as it progresses through the medium. The proof is difficult, but Brillouin and Sommerfeld showed that in a medium described by a realistic dielectric function, no signal can be propagated faster than c; for details we refer the reader to the book by Brillouin (1960), in which English translations of the original papers on this subject can be found. Subsequently, Kramers showed that a necessary and sufficient condition for the signal velocity in a medium to be less than c is that the real and imaginary parts of its refractive index satisfy the dispersion relations (2.49), (2.50); therefore, the proof of Brillouin and Sommerfeld, who used such a refractive index in their analysis, is a special case of a more general result.

The proof that the signal velocity cannot be greater than c is complicated; but it is possible to obtain some insight into refractive indices less than 1—or greater than 1 for that matter—by simple reasoning based on the oscillator model discussed above. To do so, we adopt a microscopic approach according to which the oscillators in a sample of matter are driven by an incident plane wave and reradiate (scatter) waves in all directions. In directions other than that of the incident wave, there is almost complete destructive interference of the scattered waves. In the direction of propagation, however, the incident and scattered waves combine to produce a transmitted wave with a phase either retarded or advanced relative to that of the incident wave depending on the phase difference between an oscillator and the incident wave; as shown in Fig. 9.2*a*, this relative phase can vary from 0° to 180°.

Consider the waves scattered by isotropic dipole oscillators in the thin slab of matter shown in Fig. 9.3; only part *a* is of concern at the moment. These waves add vectorially at point P to produce the resultant forward-scattered wave s; the important point, which is by no means obvious yet, is that this resultant scattered wave is phase shifted 90° relative to the incident wave (in addition to the phase shift between the oscillators and the incident wave). The background necessary to show this has been presented in Chapter 3; Fig. 3.8 is similar to Fig. 9.3 except that in the former the scatterers were arbitrary particles. The transmitted field t at P is the vector sum of the incident field and the fields scattered by all the oscillators. If we assume that the direction of vibration of the incident wave is not rotated as it propagates through the slab, the transmitted field is given by (3.39):

$$\mathbf{E}_t = E_0 e^{ikd}\left[1 - \frac{2\pi\mathcal{N}h}{k^2}(\hat{\mathbf{e}}_x \cdot \mathbf{X})_{\theta=0}\right]\hat{\mathbf{e}}_x, \tag{9.17}$$

where $\mathcal{N}$ is the number of oscillators per unit volume. This result has often been obtained using scalar diffraction theory. Strictly speaking, (9.17) only applies to a dilute collection of oscillators, but interactions among them will

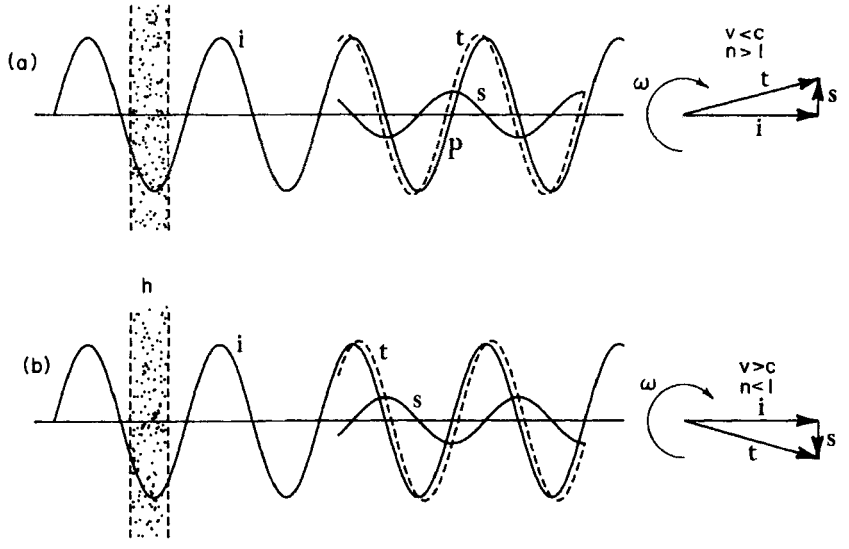

Figure 9.3 The wave transmitted (t) by a slab of dipole oscillators is the sum of incident (i) and scattered (s) waves.

not affect the qualitative aspects of our analysis, which is intended to be descriptive rather than completely rigorous. The vector scattering amplitude $\mathbf{X}$ for an isotropic dipole with polarizability α is (5.17):

$$\mathbf{X} = \frac{ik^3}{4\pi}\alpha\hat{\mathbf{e}}_r \times (\hat{\mathbf{e}}_r \times \hat{\mathbf{e}}_x).$$

Since $\hat{\mathbf{e}}_r \times \hat{\mathbf{e}}_x = \hat{\mathbf{e}}_y$ and $\hat{\mathbf{e}}_r \times \hat{\mathbf{e}}_y = -\hat{\mathbf{e}}_x$ when $\theta = 0°$, we have

$$(\hat{\mathbf{e}}_x \cdot \mathbf{X})_{\theta=0} = \frac{-ik^3}{4\pi}\alpha,$$

which can be substituted into (9.17) to obtain

$$\mathbf{E}_t = \mathbf{E}_i\left(1 + i\frac{\mathcal{N}kh\alpha}{2}\right) = \mathbf{E}_i + \mathbf{E}_s. \tag{9.18}$$

It follows from (9.5) and (9.6) that the polarizability can be written $\alpha = |\alpha|e^{i\Theta}$, where Θ is the phase difference between the displacement of an oscillator and the field that excites it. Thus, the total scattered field is

$$\mathbf{E}_s = \tfrac{1}{2}\mathbf{E}_i\mathcal{N}hk|\alpha|e^{i(\Theta+\pi/2)}, \tag{9.19}$$

where we have used $i = e^{i\pi/2}$. The significance of (9.19) is that the oscillators scatter waves that interfere at P to give a total scattered wave $\mathbf{E}_s$ which is 90° out of phase with the oscillators and Θ + 90° out of phase with the incident wave. Figure 9.3*a* shows the incident wave i, the 90° phase-shifted scattered wave s, and the transmitted wave t for low frequencies where $\Theta \simeq 0$; phasor

diagrams are included for those who are enlightened by such. Note that the transmitted wave is retarded (i.e., it *lags* the incident wave) because of interactions with all the oscillators in the slab. Interaction with successive slabs of oscillators as the wave moves through the medium results in a phase velocity less than c: $n > 1$. Figure 9.4 shows the phase relations that lead to $n > 1$ at low frequencies; on the left side of the figure the vertical scale shows the oscillator phase relative to the incident wave, and on the right side the vertical scale shows the phase of the total scattered wave relative to the incident wave; phasor diagrams are also included. At frequencies well above the resonant frequency the oscillator phase is almost 180° and the scattered wave has a phase of almost 270°. Figure 9.3*b* shows that the scattered wave *leads* the incident wave, giving a transmitted wave that is *advanced* relative to the incident wave because of interaction with the oscillators in the slab. Interaction with successive slabs of oscillators as the wave moves through the medium results in a phase velocity greater than c: $n < 1$. Such a seemingly strange effect as the speeding up of light is thus no stranger than the slowing down of light; both effects depend on the relative phase of the waves radiated by oscillators that have been set in motion by the electromagnetic field. It should be carefully noted, however, that this entire discussion has been based on the *steady-state* response of the oscillators. Consideration of the transient response would give quite different results, including "precursors" which travel through the medium at exactly c regardless of the oscillator response (see, e.g., Stratton, 1941, pp. 333–340, for a discussion of the transients leading up to the steady-state response). Thus, a pulse of electromagnetic energy would not follow the behavior we have just sketched because the steady state would not

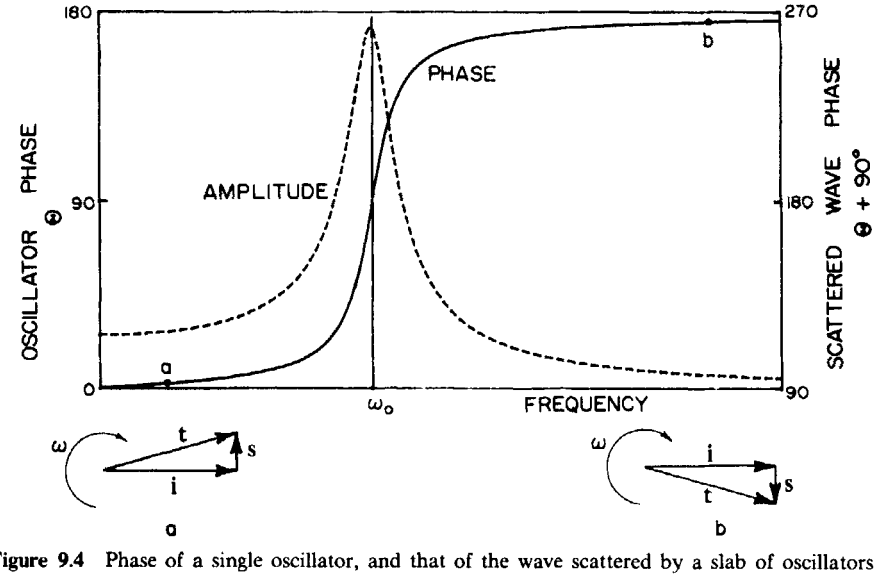

Figure 9.4 Phase of a single oscillator, and that of the wave scattered by a slab of oscillators relative to that of the wave exciting them.

have time to build up. In particular, the signal carried by the pulse could not be propagated faster than the free-space speed of light.

9.1.4 An Example of Electronic Excitations: MgO

For all solids and liquids there is a frequency region in the ultraviolet where light is strongly absorbed because the photon energy matches energy differences between filled and empty electron energy levels. Since there is a continuum of both empty and filled levels (bands), the result is an extensive region of high absorption. The gross properties of this complicated quantum system can be represented by a single classical oscillator with sufficient strength and damping to give it strong absorption over a broad frequency range. Of course, such a model cannot be expected to give the details of the electronic absorption structure, but it can give the general features. Thus, it is useful in guiding intuition and sometimes in coarse modeling of optical constants.

Our first illustrative example of a real material is the electronic excitations of MgO, an insulating crystalline solid, which will be one of the representative solids of Chapter 10. The reflectance measured at near-normal incidence over the photon energy range from about 1 to 30 eV (2 eV corresponds to a wavelength of about 0.62 μm) is shown in Fig. 9.5; these data and the corresponding optical constants are from Roessler and Walker (1967), who give a table of n and k. Peaks and valleys in the reflectance curve are caused mostly by variations in the density of occupied and vacant electron states. The optical constants derived from a Kramers–Kronig analysis of the reflectance data (see Section 2.7) are shown in the bottom part of the figure; the $1/\omega^4$ limiting behavior of the reflectance (9.15) was used to extrapolate the data to infinite energy. The dashed curves are the result of calculations based on a one-oscillator model using the parameters given in the figure caption. With these oscillator parameters the dielectric functions were calculated from (9.8) and (9.9); the corresponding optical constants n and k follow from (9.2), and the normal-incidence reflectance from (2.58).

If we disregard the fine structure, we see that the gross behavior of R, n, and k is given correctly by this simple one-oscillator model. The similarity to Fig. 9.2 is evident. At energies well below the resonance peak, which includes the visible region from about 2 to 3 eV, the material is nonabsorbing (small k), while n is almost constant, increasing only slightly toward higher energy. This behavior of n is the normal dispersion shown by all common transparent materials at visible wavelengths; it is the sort of frequency dependence one finds in elementary texts for the refractive index of glass, water, ice, and so on. In fact, this nearly constant refractive index that we have grown up with undoubtedly contributes to our collective prejudice that optical constants are really essentially constant, except for a small increase of n toward the blue, which causes separation of white light into a rainbow of colors upon passing through a prism or a water drop. Even the one-oscillator model clearly shows, however, that this prejudice is an all too simplistic view of optical properties;

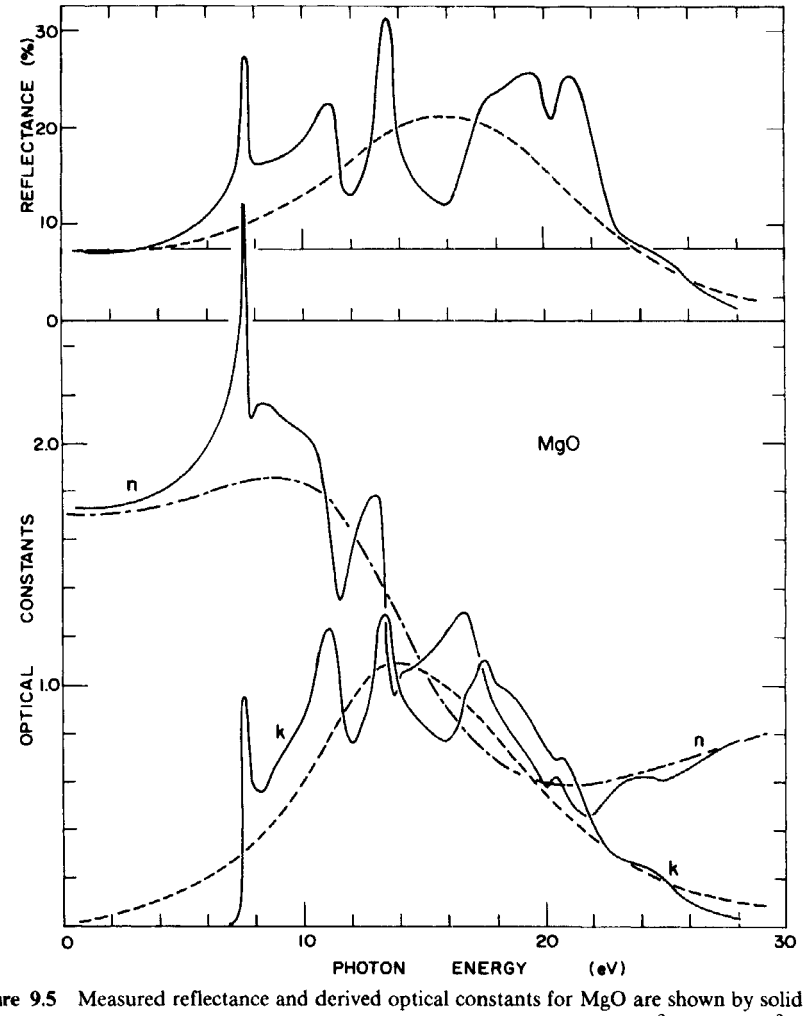

Figure 9.5 Measured reflectance and derived optical constants for MgO are shown by solid lines (Roessler and Walker, 1967). Calculations for a one-oscillator model with $\omega_p^2 = 321$ (eV)^2, $\gamma = 8$ eV, and $\omega_0 = 13$ eV are shown by dashed lines.

normal dispersion of n in the nonabsorbing region is inseparably connected with, and in a sense caused by, the strong absorption band centered at $\mathcal{E}_0 = \hbar\omega_0$. All visibly transparent solids and liquids must therefore have strong absorption in the ultraviolet where they are opaque.

In the energy region broadly centered about 14 eV ($\lambda \simeq 880$ Å), light is strongly absorbed in MgO after penetrating the surface of the crystal. We can estimate the penetration depth from (2.52): $I/I_0 = \exp(-4\pi kz/\lambda)$. For $k \simeq 1$ and $\lambda = 0.88 \times 10^{-5}$ cm, the $1/e$ penetration depth is about 10^{-6} cm, or 100 Å; thus, it would be hopeless to attempt cutting and polishing or cleaving a crystal thin enough so that transmission measurements could be made in this energy region. On the other hand, a 100-Å penetration depth corresponds to

many atomic layers in the crystal; hence, reflection is not just a phenomenon confined to surface layers of atomic dimensions, as is, for example, low-energy electron diffraction by solids.

High absorption in the far ultraviolet is accompanied by high reflectance, as was pointed out for the general oscillator model. Figure 9.5 shows that MgO reflects over 20% of normally incident light in the vicinity of 20 eV ($\lambda \simeq 600$ Å); this compares well with platinum—a common far-ultraviolet reflectance coating—which has a reflectance of about 12% at 18 eV (Hass and Tousey, 1959). Many nonconducting solids have higher reflectances in the far ultraviolet than metals. At still higher energies, of course, the reflectance goes to zero, as does k, and n approaches 1 from below; all these trends are shown in Fig. 9.5 by the measured values, which are in accord with the limiting behavior (9.14) and (9.15) predicted by the model calculations. Low reflectance in the extreme ultraviolet ($\sim$ 500 Å or less) is common for all solids: there are no efficient normal-incidence mirrors in the far ultraviolet and soft x-ray regions.

9.1.5 An Example of Lattice Vibrations: α-SiC

It was shown in the preceding section that the optical properties corresponding to electronic transitions in condensed matter are qualitatively described correctly by a one-oscillator model, although one would hesitate to use such a simple model to, for example, analyze reflectance data quantitatively. In contrast, the lattice vibrational modes in some crystals are so accurately described by simple oscillator theory that it is commonly used to determine the optical constants from measurements. Since the lattice vibrations and electronic excitations are well separated in energy for many solids, the effect of the electrons can be well approximated by the low-frequency limit (9.16). That is, at frequencies low compared with characteristic electronic excitation frequencies, the dielectric function is taken to be a real constant; with this assumption, the modified one-oscillator model appropriate to lattice vibrations is

$$\epsilon = \epsilon_{0e} + \frac{\omega_p^2}{\omega_t^2 - \omega^2 - i\gamma\omega}. \tag{9.20}$$

The notation ϵ_{0e} indicates that this is the dielectric function at frequencies low compared with *electronic* excitation frequencies. We have also replaced ω_0 with ω_t, the frequency of the *transverse* optical mode in an ionic crystal; microscopic theory shows that only this type of traveling wave will be readily excited by a photon. Note that ω_p^2 in (9.20) corresponds to $\mathcal{N}e^2/m\epsilon_0$ for the lattice vibrations (ionic oscillators) rather than for the electrons. The mass of an electron is some thousands of times less than that of an ion; thus, the plasma frequency for lattice vibrations is correspondingly reduced compared with that for electrons.

A solid for which this one-oscillator model fits extremely well is α-SiC; this is a "textbook" example, although it is a solid of considerable technological importance. Furthermore, it seems to be one of those few solids that have been

identified in the far reaches of interstellar space by means of just such vibrational absorption features presented here. Since α-SiC is not completely isotropic we should actually treat it according to the anisotropic model of Section 9.3. However, its infrared properties are almost the same for the two principal directions. For normal incidence reflectance from platelets of SiC, which tend to grow with flat faces perpendicular to the hexagonal axis, the optical properties are isotropic.

Measured normal incidence reflectances of α-SiC for incident electric field perpendicular to the hexagonal axis are shown in Fig. 9.6; these are unpublished measurements made in the authors' laboratory, but they are similar to those published by Spitzer et al. (1959). Also included in this figure are both sets of optical constants—n, k and ϵ', ϵ''—calculated from the best fit of a one-oscillator model to the experimental data. Note that the model curve is almost a perfect representation of the data over the entire range shown; for this solid, the technique of fitting data with a one-oscillator model is both a simple and accurate method for extracting optical constants.

Many of the features exhibited by the simple model (Fig. 9.2) are also seen in Fig. 9.6: normal dispersion of n on either side of the resonance frequency; a narrow region of anomalous dispersion in the neighborhood of the absorption band; and high reflectance around the absorption band with lower reflectance away from the resonance frequency where k is small. A new feature appears because ϵ_{0e} has replaced 1 in the simple oscillator equation (9.7): the region of negative ϵ' ($n < k$) is confined to a narrower region near the resonance; in contrast, ϵ' in Fig. 9.2 is negative in a greater range above the frequency near ω_0 where ϵ' crosses the ω axis. The high-frequency edge of the negative ϵ' region, where $\epsilon' = 0$, is denoted by ω_l, the *longitudinal* optical mode frequency; this is the frequency at which longitudinal oscillations of the ions are resonant. Without going into detail we can obtain some insight into this by considering the Maxwell equation

$$\nabla \cdot \mathbf{D} = \epsilon \nabla \cdot \mathbf{E} = 0.$$

If $\epsilon \neq 0$, then $\nabla \cdot \mathbf{E} = 0$ and the electric field is *transverse*. However, if $\epsilon = 0$ at some frequency, then $\nabla \times \mathbf{H} = 0$. This in turn, together with $\nabla \cdot \mathbf{B} = 0$, implies that $\mathbf{B} = 0$ and, consequently, $\nabla \times \mathbf{E} = 0$; that is, the electric field is *longitudinal*. Note then that ω_l is the frequency at which ϵ vanishes or nearly does so.

In the region between ω_t and ω_l, which for SiC is between about 800 and 1000 cm^{-1}, the reflectance is high not because of large k but because of small n. If $n \approx 0$, the normal incidence reflectance is nearly 100%; only for the undamped oscillator ($\gamma = 0$) is the reflectance actually 100%, but solids like SiC approach this rather closely. If the damping constant γ in (9.20) is set equal to zero, the real part of the dielectric function becomes

$$\epsilon' = \epsilon_{0e} + \frac{\omega_p^2}{\omega_t^2 - \omega^2}, \tag{9.21}$$

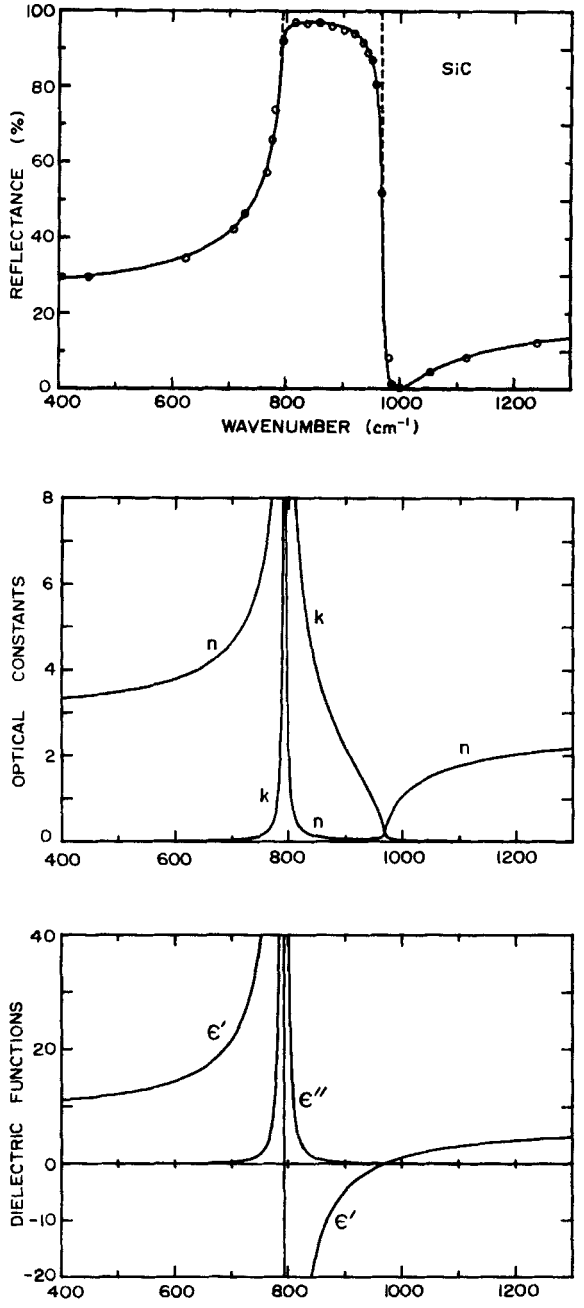

Figure 9.6 Measured reflectance (circles) of α-SiC. The solid curves are from (9.20) with $\omega_t = 793\ \text{cm}^{-1}$, $\gamma = 4.76\ \text{cm}^{-1}$, $\omega_p^2 = 2.08 \times 10^6\ \text{cm}^{-2}$, and $\epsilon_{0e} = 6.7$; the dashed curve is for the same model with $\gamma = 0$. The wave number is $1/\lambda$.

and the imaginary part ϵ'' is an infinitely sharp spike centered at ω_t. R calculated for this undamped model is shown by dashed lines in Fig. 9.6. Note that SiC is well approximated by neglecting γ, which is small compared with ω_t; in particular, the 100% theoretical reflectance between ω_t and ω_l is almost reached by the actual reflectance, which exceeds 97% in this region. Such high reflectances of ionic crystals in narrow infrared spectral regions provide means for making band-pass reflection filters, which are used in some commercial infrared spectrophotometers. The contrast between reflectances in and away from the high-reflectance region can be increased by multiple reflection: a beam of light with a continuum of infrared frequencies, upon being multiply reflected by a series of ionic crystals, will emerge with mostly frequencies in the high-reflectance region remaining. Discovery of this effect gave rise to the terminology *Reststrahlen* (residual ray) mode for this type of crystal oscillation.

An interesting and useful relation can be derived between the frequencies and the real parts of the dielectric function on either side of the *Reststrahlen* band. The frequency ω_l at which ϵ' vanishes is, from (9.21), given approximately by

$$\omega_l^2 = \omega_t^2 + \frac{\omega_p^2}{\epsilon_{0e}}. \tag{9.22}$$

For frequencies low compared with the transverse optical frequency ω_t, the dielectric function (9.21) approaches the limiting value ϵ_{0v}:

$$\epsilon_{0v} = \epsilon_{0e} + \frac{\omega_p^2}{\omega_t^2}. \tag{9.23}$$

The physical significance of ϵ_{0e} and ϵ_{0v} should be clear from Fig. 9.16. If (9.22) and (9.23) are combined we obtain the *Lyddane–Sachs–Teller relation*:

$$\frac{\omega_l^2}{\omega_t^2} = \frac{\epsilon_{0v}}{\epsilon_{0e}}. \tag{9.24}$$

9.2 THE MULTIPLE-OSCILLATOR MODEL

The one-oscillator model is quite useful in describing many optical excitations, especially when modified to include—in the low-frequency limit—the effect of all oscillators removed to higher frequencies [e.g., (9.20)]. The model becomes even more useful over a broader range of frequencies if it is extended to a multiplicity of oscillators. A naive pictorialization of the multiple-oscillator model is that it is a collection of weights and springs, as in Fig. 9.1, but of more than one type; that is, there is more than one resonant frequency. A rigorous approach to treating lattice vibrations, for example, would be to separate the motions of the electrons and the lattice ions, write down the equations of motion for the ions moving in some kind of effective potential,

expand this potential to terms of second order in the displacement of the ions from equilibrium (the *harmonic approximation*), and transform the equations of motion to a system of normal coordinates; the result is a set of independent equations of motion for effective harmonic oscillators—a collection of weights and springs. Because of the superposition principle for amplitudes in the harmonic approximation, the complex polarizability is an additive quantity, that is, summable over the effective oscillators. In general, therefore, the dielectric function for a collection of oscillators is just the sum over the various oscillators

$$\epsilon = \epsilon_0 + \sum_j \frac{\omega_{pj}^2}{\omega_j^2 - \omega^2 - i\gamma_j\omega}, \tag{9.25}$$

where the parameters of the jth oscillator are the resonant frequency ω_j, the damping constant γ_j, and the plasma frequency ω_{pj}. As in (9.20), ϵ_0 represents the effect of all oscillators well removed to higher frequencies. This is a division for convenience; if *all* oscillators are included in the summation, then $\epsilon_0 = \epsilon(\infty) = 1$. Note that n and k are not summable: they must be obtained from (9.25).

A simple application of the multiple-oscillator theory is to fit measured reflectance data for MgO in the *Reststrahlen* region. In Section 9.1 we considered the electronic excitations of MgO, whereas we now turn our attention to its lattice vibrations. A glance at the far-infrared reflectance spectrum of MgO in Fig. 9.7 shows that it does not completely exhibit one-oscillator behavior: there is an additional shoulder on the high-frequency side of the main reflectance peak, which signals a weaker, but still appreciable, second oscillator. The solid curves in Fig. 9.7 show the results of a two-oscillator calculation using (9.25); the reflectance data were taken from Jasperse et al. (1966), who give the following parameters for MgO at 295°K:

$$\epsilon_0 = \epsilon_{0e} = 3.01$$

$$\omega_1 = 401\ \text{cm}^{-1} \qquad \gamma_1 = 7.62\ \text{cm}^{-1} \qquad \frac{\omega_{p1}^2}{\omega_1^2} = 6.6$$

$$\omega_2 = 640\ \text{cm}^{-1} \qquad \gamma_2 = 102.4\ \text{cm}^{-1} \qquad \frac{\omega_{p2}^2}{\omega_2^2} = 0.045$$

Notice the second, weaker oscillator at 640 cm^{-1}; from a quantum viewpoint, this oscillator is interpreted as the excitation of two phonons by a photon. In order for momentum to be conserved, two phonons with almost equal and opposite momenta must be created: a photon has negligible momentum compared with phonon momenta. Such two-phonon transitions usually occur to a noticeable extent in ionic crystals, which necessitates a multiple-oscillator correction to the main one-oscillator *Reststrahlen* band.

We note that in MgO there is a rather large difference between the transverse optical mode frequency at about 400 cm^{-1}, where ϵ'' is a maximum,

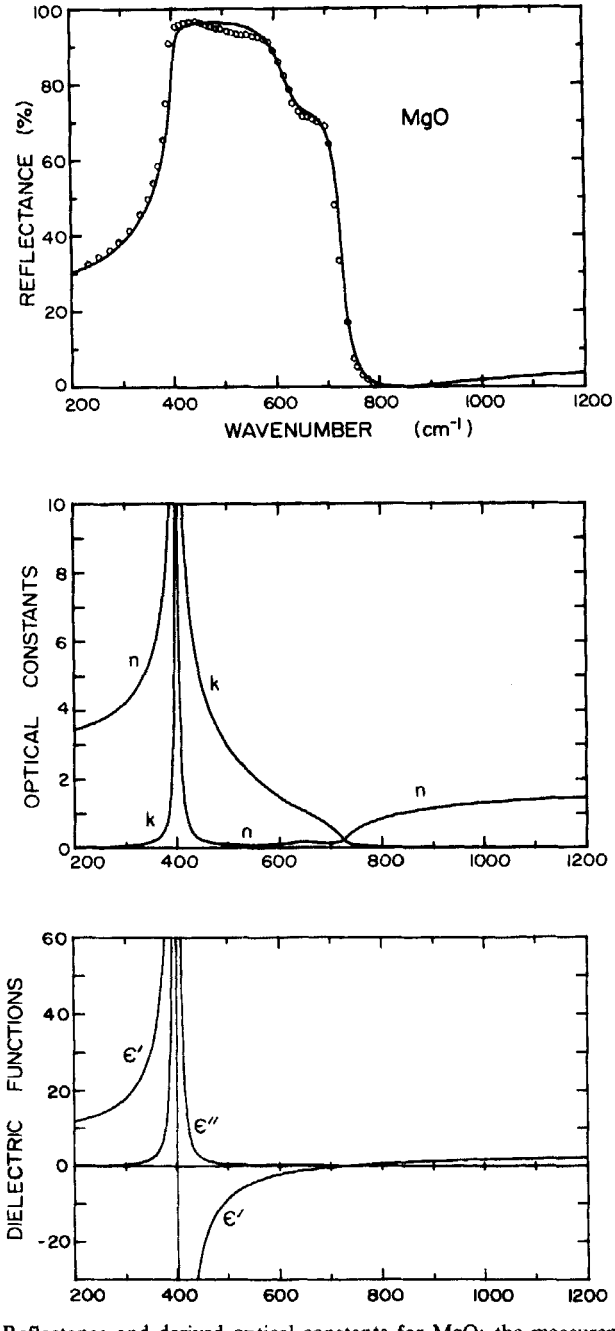

Figure 9.7 Reflectance and derived optical constants for MgO; the measurements (circles) are from Jasperse et al. (1966).

and the longitudinal optical mode frequency, where $\epsilon' = 0$. This in turn implies [see (9.24)] a large difference between the real part of the dielectric functions in the high- and low-frequency limits: $\epsilon_{0e} = 3.01$ and $\epsilon_{0v} = 9.64$. More important for absorption by small particles, the negative ϵ' region extends between ω_t and ω_l. We shall show in Chapter 12 that small particles of various shapes can absorb strongly throughout the negative ϵ' region. Because of the extent of this frequency region in MgO, its small-particle absorption spectrum can look quite different from its absorption spectrum in thin films, which is similar to the k curve.

9.3 THE ANISOTROPIC OSCILLATOR MODEL

Common liquids are optically isotropic, and the solids that physicists seem to like most are cubic and therefore isotropic. As a consequence, treatments of optical properties, particularly from a microscopic point of view, usually favor isotropic matter. Among the host of naturally occurring solids, however, most are *not* isotropic. This somewhat complicates both theory and experiment; for example, measurements of optical constants must be made with oriented crystals and polarized light. But because of the prevalence of optically anisotropic solids, we are compelled to extend the classical models to embrace this added complexity.

In the preceding sections the optical response of matter has been described by a *scalar* dielectric function ϵ, which relates the electric field $\mathbf{E}$ to the displacement $\mathbf{D}$. More generally, $\mathbf{D}$ and $\mathbf{E}$ are connected by the *tensor* constitutive relation (5.46), which we write compactly as $\mathbf{D} = \epsilon_0 \bar{\epsilon} \cdot \mathbf{E}$. The dielectric tensor $\bar{\epsilon}$ is often symmetric, so that a coordinate system can be found in which it is diagonal:

$$\bar{\epsilon} = \begin{pmatrix} \epsilon_1 & 0 & 0 \\ 0 & \epsilon_2 & 0 \\ 0 & 0 & \epsilon_3 \end{pmatrix},$$

where ϵ_1, ϵ_2, ϵ_3, are the *principal* dielectric functions. Thus, if the electric field is aligned along one of the principal axes, then $\mathbf{D}$ and $\mathbf{E}$ are parallel.

To give physical meaning to the principal dielectric functions, we consider propagation of plane waves $\mathbf{E}_0 \exp(i\mathbf{k} \cdot \mathbf{x} - i\omega t)$ in an anisotropic medium; that is, we ask: What kind of plane waves can propagate in such a medium without change of polarization? If we follow the same reasoning as in Section 2.6, we obtain from the Maxwell equations

$$\mathbf{k}(\mathbf{k} \cdot \mathbf{E}_0) - \mathbf{E}_0(\mathbf{k} \cdot \mathbf{k}) = -\frac{\omega^2}{c^2} \bar{\epsilon} \cdot \mathbf{E}_0, \qquad \mathbf{k} \cdot (\bar{\epsilon} \cdot \mathbf{E}_0) = 0,$$

where we have assumed that $\mu = \mu_0$. Let us consider the special case where $\mathbf{k}$ is along one of the principal axes, which we may take to be the z axis without loss

of generality. Then if $\mathbf{E}_0$ is referred to principal axes, the equations above reduce to

$$\left(\mathrm{k}^2 - \frac{\omega^2\epsilon_1}{c^2}\right)E_{0x} = 0, \qquad \left(\mathrm{k}^2 - \frac{\omega^2\epsilon_2}{c^2}\right)E_{0y} = 0, \qquad \epsilon_3 E_{0z} = 0.$$

If $\epsilon_3 \neq 0$, then $E_{0z} = 0$: the wave is transverse. There are two solutions to these equations:

$$\mathrm{k}^2 = \frac{\omega^2\epsilon_1}{c^2}; \qquad E_{0x} \neq 0, \quad E_{0y} = 0,$$

$$\mathrm{k}^2 = \frac{\omega^2\epsilon_2}{c^2}; \qquad E_{0x} = 0, \quad E_{0y} \neq 0.$$

Thus, plane waves can propagate along the z axis without change of polarization provided that they are either x-polarized or y-polarized. The complex refractive indices for these two types of waves, however, are different:

$$n_1 + ik_1 = \sqrt{\epsilon_1}, \qquad n_2 + ik_2 = \sqrt{\epsilon_2}.$$

If $\epsilon_1 = \epsilon_2$, then the z axis—the direction of propagation—is called the *optic axis* or the *c axis*. In this analysis we have tacitly assumed that the coordinate transformation to principal axes diagonalizes both the real and imaginary parts of the dielectric tensor.

In frequency regions where absorption is small the two indices of refraction n_1 and n_2 give rise to the phenomenon of double refraction. One of the most common uses for this property is in making wave retarders such as quarter-wave plates: incident light linearly polarized with equal x and y field components is phase shifted upon transmission because of the two different phase velocities c/n_1 and c/n_2. An entire field, usually referred to as crystal optics, arises out of this and further applications of crystal anisotropy.

Different refractive indices n for different linear polarization states of light propagating along a principal axis is called (linear) *birefringence*. Crystals with this property are said to be birefringent or doubly refracting. If there is appreciable absorption, the attenuation of a wave will also depend on polarization; this is referred to as *dichroism* or, more specifically, linear dichroism, to distinguish it from absorption differences in circularly polarized light.

The classical picture that describes these anisotropic effects based on the Lorentz model is illustrated in Fig. 9.8, which is a generalization of the spring model of Fig. 9.1; note that the spring stiffness depends on direction.

To obtain expressions for the principal dielectric functions we need only write three equations similar to (9.20) with three different sets of oscillator parameters appropriate to $\epsilon_1, \epsilon_2, \epsilon_3$. Each set of parameters corresponds to one

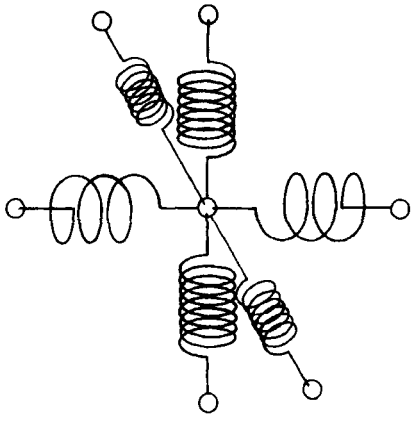

Figure 9.8 Anisotropic oscillator.

of the three different springs in Fig. 9.8. A more accurate description of the principal dielectric functions than can be given with one oscillator for each principal axis is a multiplicity of such oscillators (see Section 9.2).

The spring model suggests that the symmetry of the crystal lattice determines the different forms of the dielectric tensor; that is, they are related to the seven types of crystalline solid (amorphous solids and most liquids are isotropic). This is summarized as follows:

Isotropic. $\epsilon_1 = \epsilon_2 = \epsilon_3$

Amorphous solids
Most liquids
Cubic crystals

$$\begin{pmatrix} \epsilon' + i\epsilon'' & 0 & 0 \\ 0 & \epsilon' + i\epsilon'' & 0 \\ 0 & 0 & \epsilon' + i\epsilon'' \end{pmatrix}$$

Uniaxial Crystals. $\epsilon_1 = \epsilon_2 \neq \epsilon_3$

Tetragonal
Hexagonal
Trigonal

$$\begin{pmatrix} \epsilon_1' + i\epsilon_1'' & 0 & 0 \\ 0 & \epsilon_1' + i\epsilon_1'' & 0 \\ 0 & 0 & \epsilon_3' + i\epsilon_3'' \end{pmatrix}$$

Biaxial Crystals. $\epsilon_1 \neq \epsilon_2 \neq \epsilon_3$

Orthorhombic

$$\begin{pmatrix} \epsilon_1' + i\epsilon_1'' & 0 & 0 \\ 0 & \epsilon_2' + i\epsilon_2'' & 0 \\ 0 & 0 & \epsilon_3' + i\epsilon_3'' \end{pmatrix}$$

Biaxial Crystals

Triclinic
Monoclinic

$$\begin{pmatrix} \epsilon_1' & 0 & 0 \\ 0 & \epsilon_2' & 0 \\ 0 & 0 & \epsilon_3' \end{pmatrix} \quad \text{or} \quad \begin{pmatrix} \epsilon_1'' & 0 & 0 \\ 0 & \epsilon_2'' & 0 \\ 0 & 0 & \epsilon_3'' \end{pmatrix}$$

For the low-symmetry triclinic and monoclinic crystals the principal axes for the real and imaginary parts of the dielectric tensor are different. This makes life very complicated, and we—along with most other authors—will avoid such complications.

An example of a solid with anisotropic optical properties in the lattice vibration region is crystalline quartz, SiO_2, often found naturally as large, clear, single hexagonal crystals. Quartz is sometimes used for wave-retarding plates and has other commercial and scientific uses. Two different infrared reflectance spectra, taken from Spitzer and Kleinman (1961), are shown in Fig. 9.9. Polarized light was used in this experiment, and the crystal was oriented and cut properly for determination of the optical properties along the two principal axes. The positions of the *Reststrahlen* bands are quite different for the two polarization directions (parallel and perpendicular to

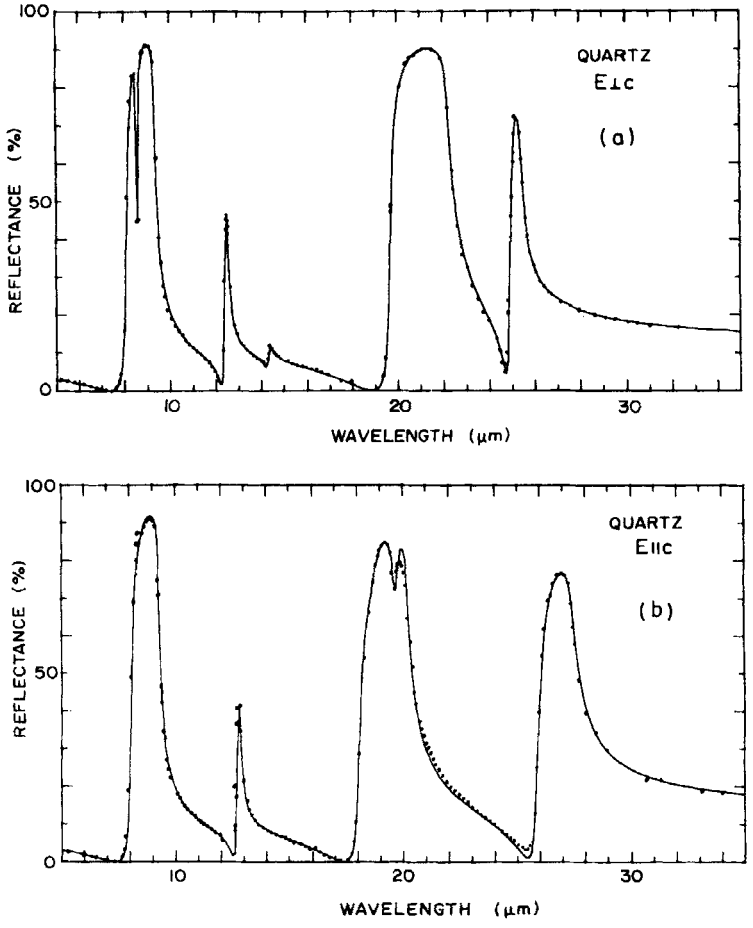

Figure 9.9 Reflectance of quartz for light polarized perpendicular (*a*) and (*b*) parallel to the *c* axis. Measurements (dots) and a theoretical fit (solid lines) are from Spitzer and Kleinman (1961).

Table 9.1 Oscillator Parameters Used to Fit the Reflectance Data Shown in Fig. 9.9 (From Spitzer and Kleinman, 1961)

ω_j (cm^{-1})	ω_{pj}^2/ω_j^2	γ_j/ω_j	
1227	0.009	0.11	
1163	0.01	0.006	
1072	0.67	0.0071	Electric field
797	0.11	0.009	perpendicular
697	0.018	0.012	to c axis
450	0.82	0.0090	
394	0.33	0.007	
	$\epsilon_{0e} = 2.356$		
1220	0.011	0.15	
1080	0.67	0.0069	
778	0.10	0.010	Electric field
539	0.006	0.04	parallel
509	0.05	0.014	to c axis
495	0.66	0.0090	
364	0.68	0.014	
	$\epsilon_{0e} = 2.383$		

the c axis), especially at wavelengths greater than about 15 μm; this shows the difference in the effective spring constants for different crystallographic directions. Spitzer and Kleinman fit the reflectance data for each polarization direction with seven oscillators, the parameters of which are given in Table 9.1. With these parameters it is an easy matter to calculate optical constants from (9.25). Comparison of calculated reflectances (solid lines) with measured reflectances (dots) shows the success of the fitting procedure; this provides an excellent quantitative illustration of the anisotropic multiple-oscillator model.

9.4 THE DRUDE MODEL

There is a marked difference between the optical properties of conductors and nonconductors of electricity; this is shown schematically in Fig. 9.10 by simple energy band diagrams. Because of the large number of electrons in a solid, there is nearly a continuum of energy states, or levels, that these electrons can occupy. However, a consequence of the periodicity of the crystal lattice is that the energy levels are grouped into *bands*. If there is a forbidden energy gap, the *band gap*, between completely filled and completely empty energy bands, the material is a nonconductor (i.e., an insulator or a semiconductor). If, on the other hand, a band of electron states is incompletely filled, or if an otherwise

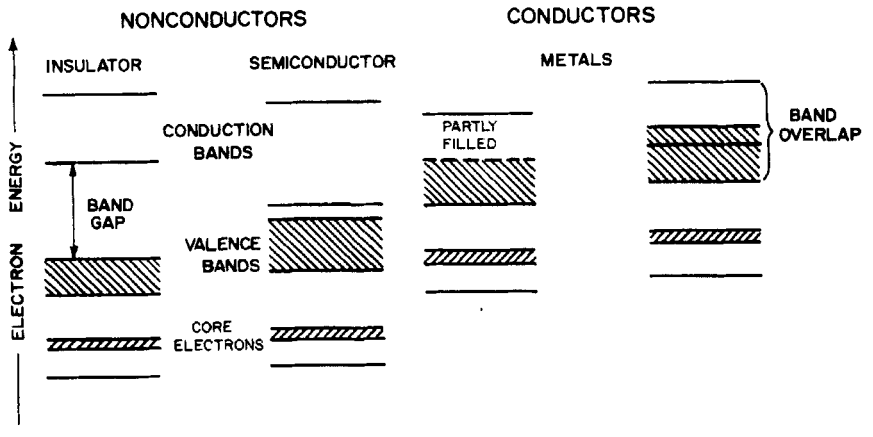

Figure 9.10 Electron energy bands in nonconductors and conductors. Filled bands are shown hatched.

filled band overlaps in energy with an empty band, the material is a conductor: electrons at the top of the energy distribution can be excited into adjacent unoccupied states by an applied electric field, which results in an electric current. This availability of vacant electron states in the same energy band provides a mechanism, *intraband* absorption, for absorption of low-energy photons. Absorption in nonconductors, *interband* absorption, is only likely for photon energies greater than the band gap. This difference between conductors and nonconductors gives rise to substantial optical differences: insulators tend to be transparent and weakly reflecting for photons with energies less than the band gap, whereas metals tend to be highly absorbing and reflecting at visible and infrared wavelengths.

Electrons in metals at the top of the energy distribution (near the Fermi level) can be excited into other energy and momentum states by photons with very small energies; thus, they are essentially "free" electrons. The optical response of a collection of free electrons can be obtained from the Lorentz harmonic oscillator model by simply "clipping the springs," that is, by setting the spring constant K in (9.3) equal to zero. Therefore, it follows from (9.7) with $\omega_0 = 0$ that the dielectric function for free electrons is

$$\epsilon = 1 - \frac{\omega_p^2}{\omega^2 + i\gamma\omega}, \tag{9.26}$$

with real and imaginary parts

$$\begin{aligned} \epsilon' &= 1 - \frac{\omega_p^2}{\omega^2 + \gamma^2}, \\ \epsilon'' &= \frac{\omega_p^2 \gamma}{\omega(\omega^2 + \gamma^2)}. \end{aligned} \tag{9.27}$$

This is the *Drude model* for the optical properties of a free-electron metal. The

plasma frequency is given by $\omega_p^2 = \mathcal{N}e^2/m\varepsilon_0$, where $\mathcal{N}$ is the density of free electrons and m is the effective mass of an electron. We have used the symbol ω_p before, but in the present context the plasma frequency has a simple physical interpretation. Let us take as our classical model of a metal a collisionless gas of free electrons moving against a fixed background of immobile positive ions. The number density $\mathcal{N}$ of positive charges is therefore constant in space and time. In equilibrium, the density of electrons is also $\mathcal{N}$. But if the electrons are disturbed slightly from equilibrium by some unspecified means, the nonuniform charge distribution will set up an electric field that will tend to restore charge neutrality. The electrons, having acquired momentum from the field, will overshoot the equilibrium configuration: there will be an oscillation. If we denote the electron number density by $\mathcal{N} - \delta\mathcal{N}$, the electric field is given by

$$\nabla \cdot \mathbf{E} = \frac{e\delta\mathcal{N}}{\varepsilon_0}. \tag{9.28}$$

If we consider only small departures from equilibrium ($|\delta\mathcal{N}/\mathcal{N}| \ll 1$), the equation of continuity is approximately

$$\nabla \cdot \mathbf{u} = \frac{\partial}{\partial t}\frac{\delta\mathcal{N}}{\mathcal{N}}, \tag{9.29}$$

where $\mathbf{u}$ is the velocity field of the electron gas, which is taken to be a continuous charged fluid. The equation of motion of this charged fluid is

$$\frac{\partial \mathbf{u}}{\partial t} + (\mathbf{u} \cdot \nabla)\mathbf{u} = -\frac{e}{m}\mathbf{E}, \tag{9.30}$$

where we neglect magnetic and pressure gradient forces. The first term on the left side of (9.30) is of order U/τ, where U is a characteristic velocity associated with the electron motion and τ is a characteristic time; the second term is of order U^2/L, where L is a characteristic length. If we assume that $1/\tau \gg U/L$, then (9.30) is approximately

$$\frac{\partial \mathbf{u}}{\partial t} = -\frac{e}{m}\mathbf{E}.$$

From these equations we obtain

$$\frac{\partial^2}{\partial t^2}\frac{\delta\mathcal{N}}{\mathcal{N}} + \omega_p^2\frac{\delta\mathcal{N}}{\mathcal{N}} = 0. \tag{9.31}$$

The existence of plane-wave solutions $\mathbf{E} = \mathbf{E}_0 \exp(i\mathbf{k} \cdot \mathbf{x} - i\omega t)$, $\delta\mathcal{N}/\mathcal{N} = C\exp(i\mathbf{k} \cdot \mathbf{x} - i\omega t)$ to (9.28) and (9.31) requires that

$$i\mathbf{k} \cdot \mathbf{E} = \frac{e\delta\mathcal{N}}{\varepsilon_0}, \tag{9.32}$$

$$C(\omega_p^2 - \omega^2) = 0. \tag{9.33}$$

There are two solutions to (9.33): (1) $\omega^2 \neq \omega_p^2, C = 0$, which implies that the

plane wave is transverse ($\mathbf{k} \cdot \mathbf{E} = 0$); and (2) $C \neq 0$, $\omega^2 = \omega_p^2$. The Drude dielectric function (9.26) vanishes at $\omega = \omega_p$ (neglecting damping); but we showed in Section 9.1 that the field is *longitudinal* at frequencies where $\epsilon(\omega) = 0$. Thus, the second solution corresponds to a longitudinal oscillation. This collective oscillation of the electron gas is called a *plasma oscillation*; it originates from long-range correlation of the electrons caused by Coulomb forces. Such plasma oscillations in gaseous discharges were investigated theoretically and experimentally by Tonks and Langmuir (1929). Further refinements were added to the classical theory by Bohm and Gross (1949ab); this work, in turn, led to a series of seminal papers on the quantum theory of plasma oscillations (Bohm and Pines, 1951, 1953; Pines and Bohm, 1952).

In the more general—and realistic—case of nonzero damping, the Drude dielectric function vanishes at the *complex* frequency $\omega_p - i\gamma/2$, provided that $\omega_p^2 \gg \gamma^2/4$. In the quantum-mechanical language of elementary excitations we refer to the excitation of a plasma oscillation as the creation (or production, or excitation) of a *plasmon*, the quantum of plasma oscillation, with energy $\hbar\omega_p$ and lifetime $\tau = 2/\gamma$. For a plasmon to be a well-defined entity, its lifetime must be sufficiently long ($\omega_p\tau \gg 1$). Although a plasmon is made up of electrons, it is *not* an electron: it is a gang, or collection, of electrons that get together under the urging of the long-range Coulomb force and decide to act in concert. Hence, for the purpose of discussing their behavior, they may, like an orchestra or a choir, be considered as a single entity following the same (Coulombic) conductor. In a choir, members are sometimes called upon to sing solos; so it is also in a collection of electrons. Individual particle behavior is exhibited, for example, in the electronic excitation spectrum of MgO (Fig. 9.5).

An elementary treatment of the free-electron motion (see, e.g., Kittel, 1962, pp. 107–109) shows that the damping constant is related to the average time τ between collisions by $\gamma = 1/\tau$. Collision times may be determined by impurities and imperfections at low temperatures but at ordinary temperatures are usually dominated by interaction of the electrons with lattice vibrations: *electron–phonon scattering*. For most metals at room temperature γ is much less than ω_p. Plasma frequencies of metals are in the visible and ultraviolet: $\hbar\omega_p$ ranges from about 3 to 20 eV. Therefore, a good approximation to the Drude dielectric functions at visible and ultraviolet frequencies is

$$\begin{aligned} \epsilon' &\simeq 1 - \frac{\omega_p^2}{\omega^2}, \\ \epsilon'' &\simeq \frac{\omega_p^2\gamma}{\omega^3}, \end{aligned} \qquad (\omega \gg \gamma). \tag{9.34}$$

These equations are identical with the high-frequency limit (9.13) of the Lorentz model; this indicates that at high frequencies all nonconductors behave like metals. The interband transitions that give rise to structure in optical properties at lower frequencies become mere perturbations on the free-electron type of behavior of the electrons under the action of an electromagnetic field of sufficiently high frequency.

The reflectance, dielectric functions, and refractive indices, together with calculations based on the Drude theory, for the common metal aluminum are shown in Fig. 9.11. Aluminum is described well by the Drude theory except for the weak structure near 1.5 eV, which is caused by bound electrons. The parameters we have chosen to fit the reflectance data, $\hbar\omega_p = 15$ eV and $\hbar\gamma = 0.6$ eV, are appreciably different from those used by Ehrenreich et al. (1963), $\hbar\omega_p = 12.7$ eV and $\hbar\gamma = 0.13$ eV, to fit the low-energy ($\hbar\omega < 0.2$ eV) reflectance of aluminum. This is probably caused by the effects of band transitions and the difference in electron scattering mechanisms at higher energies. The parameters we use reflect our interest in applying the Drude theory in the neighborhood of the plasma frequency.

For aluminum at low frequencies ϵ' is large and negative and ϵ'' is also large; the magnitude of both decreases monotonically with increasing frequency. The corresponding n and k are both large at low frequencies, but decrease toward higher frequencies; k is greater than n, which is less than 1 in much of the region below ω_p (2–15 eV). Because of the small value of n, the normal

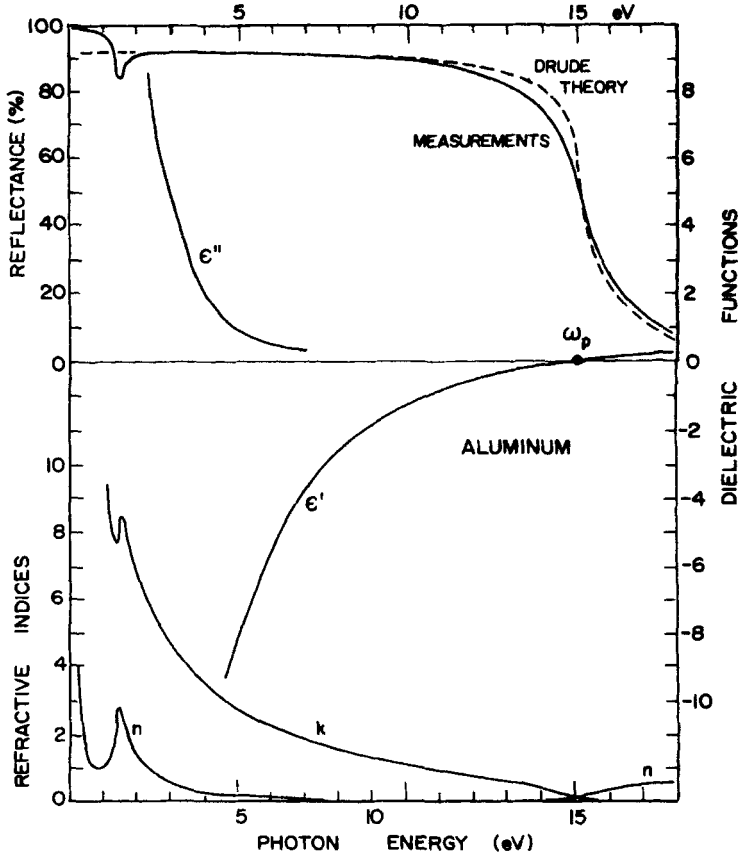

Figure 9.11 Measured reflectance of aluminum compared with the Drude theory. The dielectric function and refractive index are from Hagemann et al. (1974).

incidence reflectance is nearly 100% throughout this region, and even thin films of aluminum would transmit little light. At frequencies well above ω_p, $\epsilon' \simeq 1$ and $\epsilon'' \simeq 0$, which means that $n \simeq 1$ and $k \simeq 0$: at these frequencies, aluminum is transparent. The change from opacity to transparency near the plasma frequency is an example of *ultraviolet transparency*; it occurs in all free-electron type of metals: the alkali metals Li, Na, K, and Rb, and multivalent metals such as Mg, Al, and Pb. Ultraviolet transparency is a cut-on optical filter effect, which can be used to block light of wavelengths greater than λ_p.

We have mentioned that the region of negative ϵ' is of special importance for the optics of small particles, which can absorb and scatter strongly at frequencies that depend on their shape. In particular, strong absorption by spheres occurs at the frequency where $\epsilon' = -2$. Figure 9.11 shows that there can be an extensive region of shape-dependent absorption and scattering by small metallic particles; this will be discussed more fully in Chapter 12.

The Drude free-electron model is not limited to metals; as mentioned previously, nonconductors show a free-electron type of behavior at sufficiently high frequencies. For example, if one looks at the reflectance and dielectric functions of silicon (Philipp and Ehrenreich, 1963), one sees strong absorption bands between about 3 and 6 eV. Above about 7 eV, however, the reflectance falls smoothly from high to low values; ϵ'' goes smoothly toward zero; and ϵ' increases from a large negative value, going through zero at the plasma frequency of about 17 eV. All this is characteristic of free electrons.

Impurities in semiconductors, which release either free electrons or free holes (the absence of an electron in an otherwise filled "sea" of electrons), also give rise to optical properties at low energies below the minimum band gap (e.g., 1.1 eV for Si) that are characteristic of the Drude theory. Plasma frequencies for such doped semiconductors may be about 0.1 eV.

An interesting qualitative application of the Drude theory can be made to the ionosphere, the region of the atmosphere lying between about 50 and 500 km, in which the number density of free electrons is sufficient to affect radio-wave propagation. An electron density of 10^6 cm^{-3} gives rise to a plasma frequency of order 10^7 sec^{-1}, which corresponds to a wavelength of about 30 m. At lower frequencies (longer wavelengths) than ω_p the ionosphere is highly reflecting, just as a metal is, which has an important effect on low-frequency radio-wave propagation. The ionosphere becomes transparent to radio waves greater than ω_p for the same reason that free-electron metals become transparent in the ultraviolet. Therefore, high-frequency radio waves are not so greatly affected by "skipping" or reflection from the ionosphere. Obviously, radio communication with satellites or spaceships above the ionosphere must rely on frequencies greater than its maximum plasma frequency. The electron density is not uniform with height and varies considerably because of such changing effects as sunspot activity; also, the earth's magnetic field complicates the propagation of radio waves in the ionosphere. Nevertheless, the Drude model gives a qualitative description that helps in understanding the observed phenomena.

Table 9.2 Plasma Frequencies and Corresponding Wavelengths for a Range of Free-Electron Densities

$\mathcal{N}$ (cm^{-3})	ω_p (sec^{-1})	λ_p	Type of Plasma	
10^{24}	5.7×10^{16}	330 Å		
10^{22}	5.7×10^{15}	3300 Å	metals	Al(λ_p = 830 Å)
10^{20}	5.7×10^{14}	3.3 μm		Cs(λ_p = 3620 Å)
10^{18}	5.7×10^{13}	33 μm		doped semiconductors
10^{17}	1.8×10^{13}	105 μm	electron–hole droplets	
10^{16}	5.7×10^{12}	330 μm		
10^{6}	5.7×10^{7}	33 m	ionosphere (F layer)	
10^{5}	1.8×10^{7}	105 m		

Plasma frequencies and the corresponding wavelengths for a range of free-electron densities are given in Table 9.2; the plasma effects mentioned in this section are noted beside the wavelengths (electron–hole droplets will be discussed in Chapter 12).

9.4.1 Free and Bound Electrons in Metals

Despite its applicability to metals such as aluminum, Drude theory alone does not accurately describe the optical characteristics of many other metals. Silver is a good example of a metal that exhibits some free-electron type of behavior, which can be treated with the Drude theory; but it also has a substantial bound-electron component, which appreciably alters the free-electron optical properties. The normal-incidence reflectance of silver (Irani et al., 1971) is shown in Fig. 9.12*a*; a logarithmic scale was used to emphasize the unusually large variation of reflectance over a narrow range around ω_p. The low-energy part of the spectrum suggests a free-electron type of reflectance: it is almost 100% and falls precipitously to quite low values near the plasma frequency at about 3.9 eV. Beyond the plasma frequency, however, results differing markedly from Drude theory occur as the reflectance rises abruptly and vacillates a little before again falling to low values; this behavior above 4 eV is interpreted as a bound charge effect. In Fig. 9.12*b* the experimentally determined ϵ' for silver is decomposed into components contributed by free and bound charges. That is, polarizabilities and, hence, susceptibilities are additive; thus, we may write a composite dielectric function $\epsilon = \epsilon_f + \delta\epsilon_b$ that includes a contribution $\delta\epsilon_b$

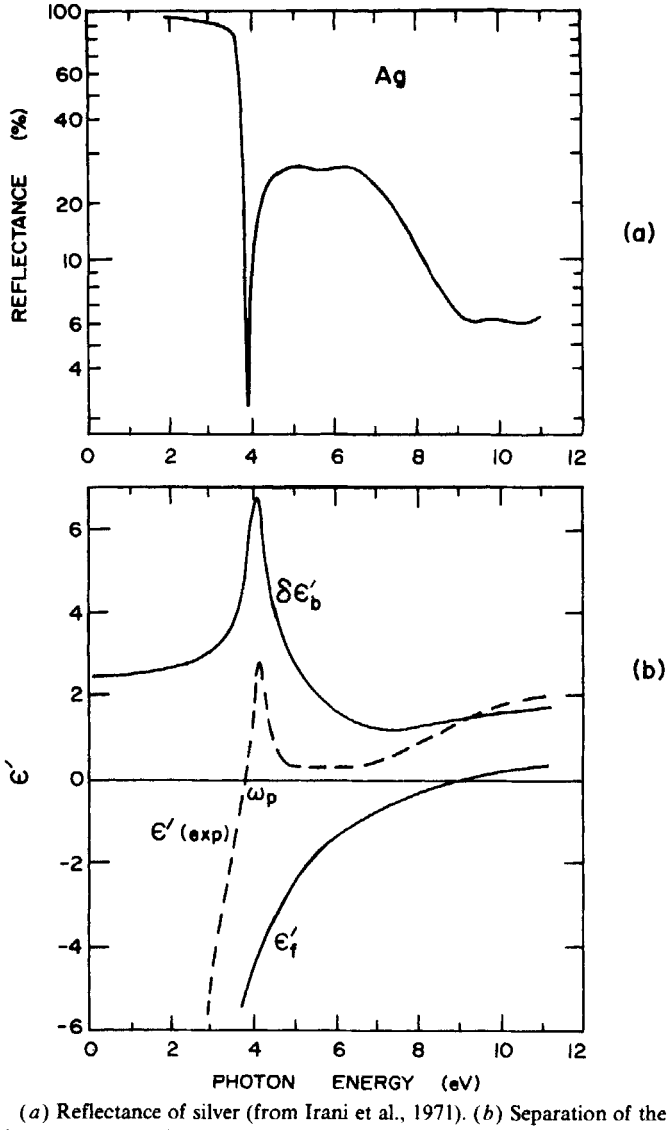

Figure 9.12 (*a*) Reflectance of silver (from Irani et al., 1971). (*b*) Separation of the measured ϵ' into free and bound contributions (from Ehrenreich and Philipp, 1962).

from Lorentz oscillators and a free-electron contribution ϵ_f:

$$\epsilon = 1 - \frac{\omega_{pe}^2}{\omega^2 + i\gamma_e\omega} + \sum_j \frac{\omega_{pj}^2}{\omega_j^2 - \omega^2 - i\gamma_j\omega},$$

where the subscript e is appended to free-electron parameters.

The free-electron contribution to the dielectric function in Fig. 9.12*b* is obtained from the Drude theory with parameters determined from the low-

frequency limit of the data ($\hbar\omega < 0.1$ eV); the bound-charge contribution then follows simply by subtraction: $\delta\epsilon_b' = \epsilon' - \epsilon_f'$. These results clearly show the strong effect of bound charges on the plasma frequency. From the equation $\omega_p^2 = \mathcal{N}e^2/m\epsilon_0$ with the electron density $\mathcal{N}$ appropriate to silver, the plasma frequency is calculated to be 9.2 eV, the frequency at which ϵ' would be approximately zero if only free electrons determined the optical properties of silver. However, the appreciable positive contribution of the bound charges at energies below about 6 eV pulls up the ϵ' curve so that it crosses the axis at 3.9 eV rather than 9 eV. The plasma frequency, defined as the frequency at which $\epsilon' = 0$, is shifted from the far to the near ultraviolet because of the bound charges, resulting in the onset of ultraviolet transparency near 3200 Å instead of 1300 Å. Almost as soon as the reflectance drops at the plasma frequency, however, the peak in $\delta\epsilon_b'$ near 4 eV causes a rise in reflectance that would not occur were it not for the bound charges. We thus see how competing bound and free charges in metals can greatly alter their optical properties.

An interesting metal to compare with silver is copper: its reddish-brown color obviously signals considerable differences in optical constants in the visible; yet the electron energy band structures of the two metals are qualitatively quite similar. The difference in their appearance lies in the position of the ϵ' peak caused by bound charges, which is near 4 eV in silver and near 2 eV in copper. Because the free-electron contribution to ϵ' is so strongly negative, the positive contribution of the bound charges is not sufficient to raise ϵ' to positive values and thereby decrease the plasma frequency, as it does in silver. Although the reflectance does not drop because the plasma frequency is shifted, the bound charges do have an important effect. The onset of their effects near 2 eV causes a sharp decrease in reflectance from nearly 100% at lower energies; a weaker example of the reflectance decrease caused by bound charges can be seen near 1.5 eV in the aluminum reflectance spectrum of Fig. 9.11. At 2 eV, which corresponds to wavelengths in the red part of the visible spectrum, the reflectance of copper is still high; at the other end of the visible spectrum (about 3 eV), the bound charges greatly reduce the reflectance. It is this higher reflectance in the red than in the blue that gives the metal its characteristic "copper" color.

9.5 THE DEBYE RELAXATION MODEL

There is another important mechanism for polarizing matter containing *permanent*, as opposed to induced, electric dipoles: partial alignment of the dipoles along the electric field against the counteracting tendency toward disorientation caused by thermal buffeting. The restoring "force" that tries to return a polarized region to an unpolarized state is thus the statistical tendency toward random orientation of the dipoles; this is quite different from the conceptual springs of the Lorentz theory. The dipole restoring tendency does not cause

overshoot leading to oscillation of the electric polarization; it is as if permanent electric dipoles are *overdamped*, whereas Lorentz oscillators are *underdamped*. Because the permanent dipoles merely relax to equilibrium, this mode of polarization is referred to as *relaxation* and is usually associated with Debye, who did the early definitive work (one of the best references continues to be *Polar Molecules*, 1929, by Debye). Since many liquids are composed of molecules that have permanent dipole moments, Debye relaxation by molecular rotation plays an important role in determining the optical constants of these liquids at certain frequencies, usually in the microwave region. Many solids also show Debye relaxation because of the presence of charged defects or impurities, which may have nonequivalent positions in the crystal lattice, leading to the possibility of reorientation of the resulting dipole moments.

The return to equilibrium of a polarized region is quite different in the Debye and Lorentz models. Suppose that a material composed of Lorentz oscillators is electrically polarized and the static electric field is suddenly removed. The charges equilibrate by executing damped harmonic motion about their equilibrium positions. This can be seen by setting the right side of (9.3) equal to zero and solving the homogeneous differential equation with the initial conditions $x = x_0$ and $\dot{x} = 0$ at $t = 0$; the result is the damped harmonic oscillator equation:

$$x = \mathrm{Re}\{x_0 e^{-i\omega_0 t} e^{-\gamma t}\}.$$

The decay of the initial polarization is therefore

$$P_l(t) = P_l(0) e^{-\gamma t} \cos(\omega_0 t);$$

we append l to the polarization to indicate a collection of Lorentz oscillators. In contrast with these damped harmonic oscillators, a collection of Debye oscillators (permanent dipoles), if polarized initially, returns to equilibrium with the time dependence

$$P_d(t) = P_d(0) e^{-t/\tau}. \tag{9.35}$$

There is no oscillation: the polarization merely relaxes toward zero with a time constant τ. In the following paragraphs, we shall use (9.35), the basic assumption of the Debye theory, to derive an expression for the dielectric function of a collection of permanent dipoles.

If at time t_0 a constant electric field E_0 (i.e., a step function) is suddenly applied to a sample of polarizable matter, the polarization will follow the time evolution illustrated schematically in Fig. 9.13. There are contributions to the polarization from electrons, lattice ions, and permanent dipoles. We shall assume that the response of the permanent dipoles is much slower than that of the electrons and ions; that is, the response of the latter may be considered to occur instantaneously compared with the time required for the matter to reach

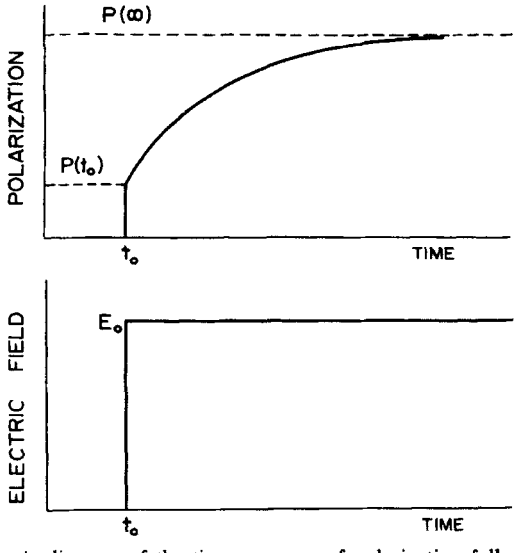

Figure 9.13 Schematic diagram of the time response of polarization following application of a field E_0 at time t_0.

its final equilibrium polarization. When the field is applied at time t_0, therefore, a polarization $P(t_0) = \varepsilon_0 \chi_{0v} E_0$ is instantaneously induced; as time increases, the polarization approaches the limiting value $P(\infty) = \varepsilon_0 \chi_{0d} E_0$. We remind the reader that in our notation χ_{0v} is the susceptibility at frequencies low compared with characteristic lattice vibrational frequencies, which are in turn low compared with electronic frequencies; and χ_{0d} is the susceptibility at frequencies low compared with dipole frequencies (i.e., the static, or dc, susceptibility). By assuming an exponential approach to equilibrium as in (9.35) we can write a physically plausible expression for the time-dependent polarization:

$$P(t) = P(\infty) - Ce^{-(t-t_0)/\tau} \qquad (t > t_0). \tag{9.36}$$

The constant C is determined from the requirement that $\lim_{t \downarrow t_0} P(t) = P(t_0)$:

$$C = P(\infty) - P(t_0) = P(t_0)(\chi_{0d} - \chi_{0v})/\chi_{0v}.$$

With a bit of rearranging (9.36) can be put in a form which is easier to interpret and which will enable us to generalize it to a series of step functions:

$$P(t) = \varepsilon_0 \chi_{0v} E_0 + \varepsilon_0 (\chi_{0d} - \chi_{0v})[1 - e^{-(t-t_0)/\tau}] E_0. \tag{9.37}$$

The first term on the right side of (9.37) is the contribution to the total

polarization from the lattice ions; the second term $P_d(t)$, is the contribution from the permanent dipoles.

Suppose now that two different two-step fields are applied: (1) at t_0 the electric field $2E_1$ is turned on and at t_1 the field suddenly changes to E_1; and (2) the field at t_1 is the same as in (1) but between t_0 and t_1 it is $E_1/2$. It is clear from Fig. 9.14 that the polarization in these two cases is different, even for $t > t_1$ when the applied field is the same; that is, the polarization at time t depends on the history of the applied field and not merely its instantaneous value. This is a specific example of a general conclusion that we made about the response of a linear medium to a time-dependent electric field (see Section 2.3). The polarization at all times greater than t_1 can be obtained by following reasoning similar to that which led to (9.37): we write $P(t)$ in the form (9.36) and require that $\lim_{t \downarrow t_1} P(t) = P_d(t_1) + \varepsilon_0 \chi_{0v} E_1$; the result is

$$P(t) = \varepsilon_0 \chi_{0v} E_1 + \varepsilon_0(\chi_{0d} - \chi_{0v}) E_1[1 - e^{-(t-t_1)/\tau}]$$

$$+ \varepsilon_0(\chi_{0d} - \chi_{0v}) E_0[e^{-(t-t_1)/\tau} - e^{-(t-t_0)/\tau}] \qquad (t > t_1). \quad (9.38)$$

It is not difficult to show that (9.38) can be written

$$P(t) = \varepsilon_0 \chi_{0v} E_1 + \varepsilon_0(\chi_{0d} - \chi_{0v}) \int_{t_0}^{t} E(t') \frac{d}{dt'} [e^{-(t-t')/\tau}]\, dt'. \quad (9.39)$$

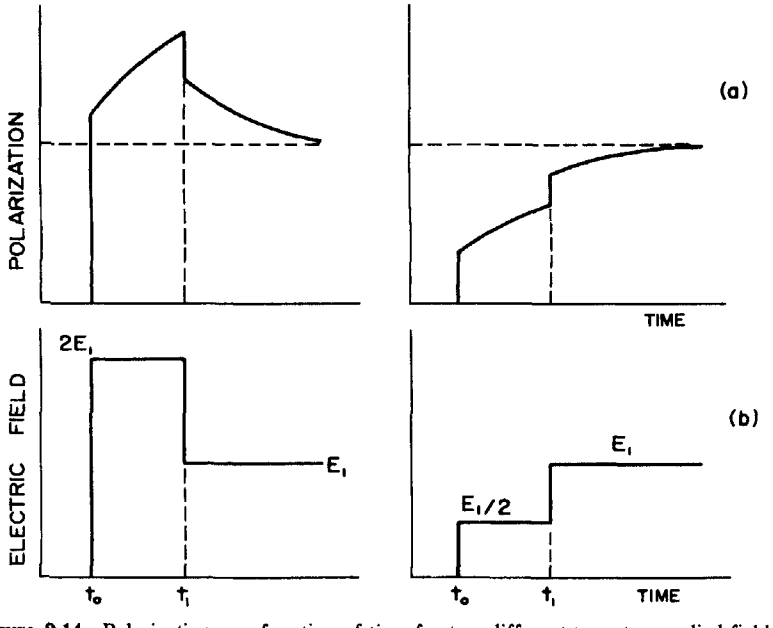

Figure 9.14 Polarization as a function of time for two different two-step applied fields.

Although this was obtained for a series of two step functions, it should be clear that it is valid for any number of such functions. Indeed, any field can be approximated by a series of step functions, where the error can be made arbitrarily small by choosing sufficiently small steps; thus, (9.39) is valid for any field. The technique of representing an arbitrary forcing function by a series of steps (or, more correctly, impulses) was first developed by Green, and a good account of this is given by Marion (1970, p. 139); the exponential function multiplying $E(t')$ in (9.39) is therefore the *Green's function* for the system of permanent dipoles in the Debye theory. The first term in (9.39) is the lattice polarization, which we assume follows the instantaneous field; the second term is the sum of all polarization changes caused by the slow dipole relaxation mechanism. Note that (9.39) is a particular example of a linear, causal constitutive relation (Section 2.3).

To obtain the frequency-dependent susceptibility $\chi(\omega)$, we need the polarization in response to a time-harmonic field $E_0 e^{-i\omega t}$:

$$P(t) = \varepsilon_0 \chi E_0 e^{-i\omega t} = \varepsilon_0 \chi_{0v} E_0 e^{-i\omega t} + \varepsilon_0 (\chi_{0d} - \chi_{0v}) \int_{-\infty}^{t} E_0 e^{-i\omega t'} \frac{d}{dt'} [e^{-(t-t')/\tau}]\, dt'. \tag{9.40}$$

Implicit in (9.40) is the assumption that ω is small compared with lattice vibrational frequencies. The susceptibility in the frequency region where Debye relaxation is the dominant mode of polarization is therefore

$$\chi = \chi_{0v} + \frac{\Delta}{1 - i\omega\tau}, \qquad \Delta = \chi_{0d} - \chi_{0v}$$

from which follows the dielectric function

$$\epsilon = \epsilon_{0v} + \frac{\Delta}{1 - i\omega\tau} \tag{9.41}$$

with real and imaginary parts

$$\epsilon' = \epsilon_{0v} + \frac{\Delta}{1 + \omega^2\tau^2}, \qquad \epsilon'' = \frac{\omega\tau\Delta}{1 + \omega^2\tau^2}. \tag{9.42}$$

Our derivation of (9.41) follows closely that of Gevers (1946) and is similar to that of Brown (1967, pp. 248–255). Because of the nature of this derivation it should hardly be necessary to do so, but it can be shown directly by integration—more easily than for the Lorentz oscillator—that the real and imaginary parts of the Debye susceptibility satisfy the Kramers–Kronig relations (2.36) and (2.37).

The imaginary part of the dielectric function (9.41) is a maximum at $\omega = 1/\tau$ and behaves similarly to ϵ'' for the Lorentz oscillator. The real part,

however, behaves quite differently: it has no maxima and no minima but decreases monotonically from ϵ_{0d} at low frequencies to ϵ_{0v} at high frequencies; the transition occurs in the neighborhood of $\omega = 1/\tau$. At low frequencies, the permanent dipoles easily follow the electric field changes, and the dc dielectric function can be quite large; at high frequencies, however, they are unable to keep up with the oscillating field, and ϵ' falls to a value that does not include a contribution from the permanent dipoles.

The Debye equations (9.42) are particularly important in interpreting the large dielectric functions of polar liquids; one example is water, the most common liquid on our planet. In Fig. 9.15 measured values of the dielectric functions of water at microwave frequencies are compared with the Debye theory. The parameters ϵ_{0d}, ϵ_{0v}, and τ were chosen to give the best fit to the experimental data; $\tau \simeq 0.8 \times 10^{-11}$ sec follows immediately from the frequency at which ϵ'' is a maximum; $\epsilon_{0d} - \epsilon_{0v}$ is $2\epsilon''_{\max}$.

On physical grounds, relaxation of permanent dipoles is expected to be highly dependent on temperature; this is in contrast with Lorentz oscillators, the dielectric behavior of which is relatively insensitive to changes in temperature. Debye (1929, Chap. 5) derived a simple classical expression for the relaxation time of a sphere of radius a in a fluid of viscosity η:

$$\tau = \frac{4\pi\eta a^3}{k_B T}, \tag{9.43}$$

where T is the absolute temperature and k_B is Boltzmann's constant. Two

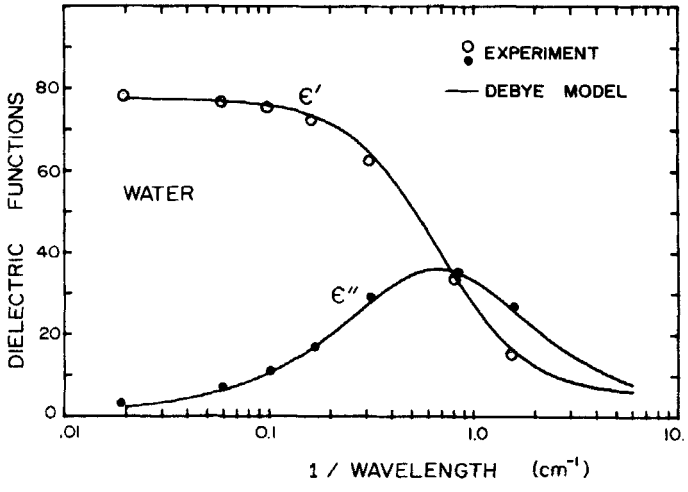

Figure 9.15 Dielectric function of water at room temperature calculated from the Debye relaxation model with $\tau = 0.8 \times 10^{-11}$ sec, $\epsilon_{0d} = 77.5$, and $\epsilon_{0v} = 5.27$. Data were obtained from three sources: Grant et al. (1957), Cook (1952), and Lane and Saxton (1952).

factors conspire to affect the relaxation time: the numerator of (9.43) arises from the viscous restoring torque on a small sphere; the denominator arises from the thermal buffeting. The greater is T, the lower the viscosity (in liquids) and the shorter the relaxation time; the greater is T, the more quickly will thermal motion randomize an oriented collection of permanent dipoles after the orienting field is removed. The room temperature viscosity of water is about 0.01 g/cm-sec, and if we take $a \simeq 10^{-8}$ cm, (9.43) yields a relaxation time of about 0.3×10^{-11} sec; thus, the simple theory is in good agreement with the relaxation time deduced from the experimental data of Fig. 9.15.

A naive interpretation of the phase transition from liquid to solid water as the temperature is decreased is that the water undergoes a large discontinuous increase in viscosity. Thus, the permanent electric dipoles that were free to rotate in the liquid are suddenly immobilized. Consistent with this interpretation is the expectation that the relaxation time for ice should be much greater than for water, with a corresponding decrease in the frequency at which ϵ'' is a maximum. This is indeed so: if water were to freeze suddenly from room temperature, then ϵ' at frequencies in the region shown in Fig. 9.15 would plunge from a high of about 80 to a low of about 3.2. Such large changes can be observed, for example, in radar backscattering from melting ice particles or freezing water droplets; this large difference between the dielectric functions of ice and liquid water is the major contributor to the "bright band" in vertical radar reflectivity profiles observed by meteorologists (see, e.g., Battan, 1973, p. 190).

Dipole relaxation is often described by a superposition of exponentially decaying functions with different relaxation times in place of the single relaxation time in (9.35). This is analogous to the need for several oscillator parameters in the Lorentz model. Both ϵ' and ϵ'' are functions of frequency; therefore, frequency can be eliminated to give a functional relationship between them. Experimental measurements of the dielectric functions in the dipole frequency region are often displayed as a plot of ϵ'' versus ϵ', called the *Cole–Cole plot*. From a glance at such a plot it is immediately obvious whether or not a single relaxation time is sufficient to determine the frequency dependence of the dielectric function; it is not difficult to show from (9.42) that for a single relaxation time, the Cole–Cole plot is a semicircle centered on the ϵ' axis at $(\epsilon_{0d} + \epsilon_{0v})/2$ and with radius $(\epsilon_{0d} - \epsilon_{0v})/2$:

$$\left[\epsilon' - \tfrac{1}{2}(\epsilon_{0d} + \epsilon_{0v})\right]^2 + \epsilon''^2 = \left[\tfrac{1}{2}(\epsilon_{0d} - \epsilon_{0v})\right]^2.$$

9.6 GENERAL RELATIONSHIP BETWEEN ϵ' AND ϵ''

We must reemphasize that the real and imaginary parts of the complex dielectric function (and the complex refractive index) are not independent. Arbitrary choices of ϵ' and ϵ'' (or n and k) do not necessarily correspond to

any real solid or liquid at some wavelength. The interdependence of ϵ' and ϵ'' has been illustrated in each of the classical models of this chapter: the Lorentz model, the Drude model, and the Debye model. These connections between real and imaginary parts of the same complex function are specific examples of the Kramers–Kronig relations discussed in Section 2.3. For any solid or liquid the real part of the dielectric function at any frequency ω is related to the imaginary part at all frequencies by

$$\epsilon'(\omega) = 1 + \frac{2}{\pi} P \int_0^\infty \frac{\Omega \epsilon''(\Omega)}{\Omega^2 - \omega^2} d\Omega. \tag{9.44}$$

We are now in a position to better understand and, we hope, appreciate, the sometimes mysterious Kramers–Kronig relations.

First, we note that the consequence of no absorption ($\epsilon'' = 0$) at all frequencies is that the integral in (9.44) vanishes and $\epsilon' = 1$. Optically, such a material does not exist: there is no way that it can be distinguished from a vacuum by optical means. The Kramers–Kronig relations also tell us that it is a contradiction to assert that either the real or imaginary parts of the dielectric function can be independent of frequency; the frequency dependence of the one implies the frequency dependence of the other. These consequences of the Kramers–Kronig relations are almost trivial, but it is disturbing how often they are blithely ignored.

The high- and low-frequency behavior of ϵ' can be inferred from (9.44) regardless of the nature and number of absorption features in ϵ''. As ω becomes arbitrarily large, all contributions to the integral go to zero and

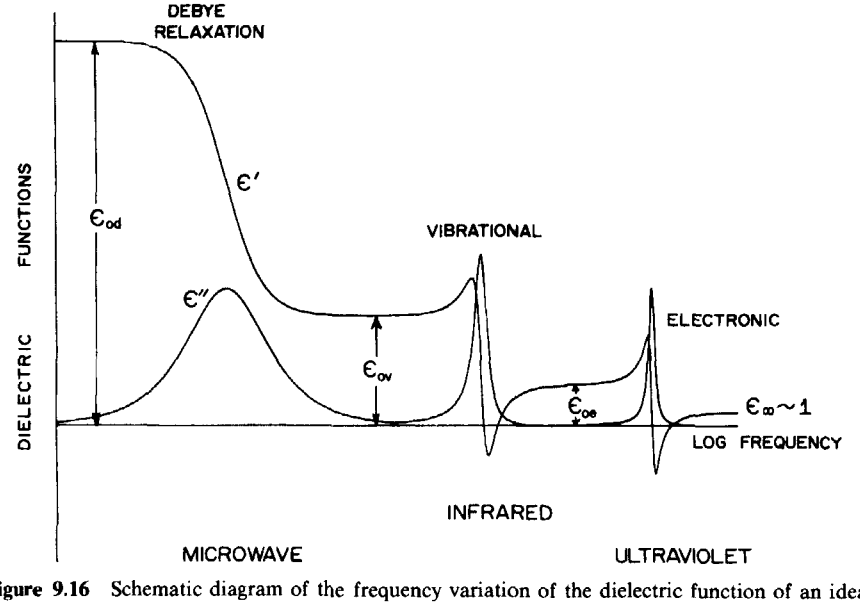

Figure 9.16 Schematic diagram of the frequency variation of the dielectric function of an ideal nonconductor.

$\lim_{\omega \to \infty} \epsilon'(\omega) = 1$. Thus, it is a general result that at frequencies far above all absorption bands ϵ' approaches the free-space value 1; the frequency is so high that none of the polarization mechanisms can respond. At low frequencies, on the other hand, ϵ' is the sum of contributions from each polarization mechanism—electronic, vibrational, and dipolar—with the lowest-frequency mechanism contributing most:

$$\epsilon'(0) = 1 + \frac{2}{\pi} \int_0^\infty \frac{\epsilon''(\Omega)}{\Omega} d\Omega. \tag{9.45}$$

The consequence of (9.45) is that for any material other than free space, somewhere at higher frequencies there must be an absorption mechanism lurking.

A schematic diagram of the frequency dependence of ϵ' and ϵ'' for an ideal nonconductor (no Drude term) is given in Fig. 9.16; this summarizes several of the points made in this chapter. Possible fine structure in the optical constants is ignored for simplicity. The notation we have used for the high- and low-frequency dielectric functions in the various models will become clearer after consulting this figure. At $\omega = 0$ the dielectric function is composed of contributions from permanent dipoles, vibrational oscillators, and electronic oscillators. As the frequency is increased, the permanent dipoles cannot respond and ϵ' drops from the static value ϵ_{0d} to ϵ_{0v}, the value at frequencies low compared with characteristic vibrational frequencies. As ω increases through the vibrational region, ϵ' oscillates and then settles down to ϵ_{0e}, the low-frequency limit for electronic modes. Finally, as the frequency increases beyond the point where all the electronic modes are exhausted, ϵ' approaches 1. In each frequency interval where ϵ' is changing there is an associated peak in ϵ'', the absorptive part of the dielectric function. There are other polarization modes associated with core electrons in the atoms, which give rise to much weaker variations in ϵ' and ϵ'' at x-ray frequencies; we have arbitrarily chosen to exclude these from our discussion of "optical properties."

NOTES AND COMMENTS

Hodgson (1970) and Christy (1972) have treated optical properties of matter in a spirit similar to that of this chapter. And so has Garbuny (1965), although within a book of broader scope.

We direct the reader to the book by Davies (1969) for further reading about wave propagation in the ionosphere.

Crystal optics—the optics of anisotropic media—is treated at an elementary level by Wood (1977). More advanced treatises are those by Nye (1957) and by Ramachandran and Ramaseshan (1961).

Fröhlich and Pelzer (1955) determined the frequencies of longitudinal waves in matter described by the three simple dielectric functions—Lorentz, Drude, and Debye—discussed in this chapter.